2016-07-01

Computational Studies of Alkane C-H Functionalization by Main-Group Metals

Samantha Jane Gustafson
Brigham Young University

Computational Studies of Alkane C–H Functionalization by Main–Group Metals

Samantha Jane Gustafson

A dissertation submitted to the faculty of
Brigham Young University
in partial fulfillment of the requirements for the degree of

Doctor of Philosophy

Daniel H. Ess, Chair
Merritt B. Andrus
Roger G. Harrison
Matt A. Peterson
Kara J. Stowers

Department of Chemistry and Biochemistry

Brigham Young University

July 2016

ABSTRACT

Computational Studies of Alkane
C–H Functionalization by
Main–Group Metals

Samantha Jane Gustafson
Department of Chemistry and Biochemistry, BYU
Doctor of Philosophy

The most efficient homogeneous catalysts for hydroxylation of light alkanes utilize transition metals in superacid solvent and operate by tandem electrophilic C–H activation/metal–alkyl (M–R) functionalization. An emerging alternative strategy to transition metals is the use of high-oxidation state main-group metals (e.g. Tl^{III}, Pb^{IV}, I^{III}) that hydroxylate light alkanes. This dissertation reports density-functional theory calculations that reveal the mechanisms, reactivity, and selectivity of Tl^{III} promoted alkane C–H functionalization in trifluoroacetic acid and Tl^{III}–dialkyl functionalization in water. Calculations reveal that Tl^{III} oxidizes alkanes via a closed-shell C–H activation and M–R functionalization mechanism that is similar to transition-metal C–H functionalization mechanisms. Comparison of Tl^{III} to similar transition metals reveals that while Tl^{III} and transition metals can have similar activation barriers for C–H activation, Tl^{III} M–R functionalization is significantly faster due to a highly polar Tl–C bond and large Tl^{III}/Tl^{I} reduction potential. The combination of a moderate C–H activation barrier combined with a low M–R functionalization barrier is critical to the success for Tl^{III} promoted alkane C–H oxidation. The proposed Tl^{III} C–H activation/M–R functionalization mechanism also provides an explanation for ethane conversion to a mixture of ethyl trifluoroacetate and ethane-1,2-diyl bis(2,2,2-trifluoroacetate). The reactivity of Tl^{III} contrasts the lack of alkane oxidation by Hg^{II}. The C–H activation transition state and frontier-orbital interactions provide a straightforward explanation for the higher reactivity of Tl^{III} versus Hg^{II}. This frontier-orbital model also provides a rationale for why the electron-withdrawing group in EtTFA provides “protection” against overoxidation. Calculations also reveal that Tl^{III}–dialkyl functionalization by inorganic Tl^{III} in water occurs by alkyl group transfer to form a Tl^{III}–monoalkyl complex that is rapidly functionalized.

Keywords: Main-Group Metal, Alkane, C–H Activation, Thallium, Trifluoroacetic acid.

ACKNOWLEDGEMENTS

First and foremost, I would like to thank my Savior Jesus Christ for the blessings and inspiration I received to complete this work. I would like to thank the Department of Chemistry and Biochemistry for awarding me the Bradshaw Organic Chemistry Fellowship. Janet Fonoimoana and the staff of department have been such a magnificent help, and I would like to express my gratitude for their tireless assistance and encouragement. My success is in large part due to the assistance of Dr. Daniel H. Ess and I am grateful for the opportunity to work with him, his countless hours of teaching and assistance, helping me to stretch, his patience, and helping me to succeed. I am thankful for the assistance Dr. Kara J. Stowers, Roger G. Harrison, Merritt B. Andrus, and Matt A. Peterson for the time and effort they spent serving on my committee and helping me to be successful. I am grateful for all other professors that have given me instruction at BYU. I would also like to give thanks to the Fulton Supercomputing Computing facility for access to the supercomputers and assistance from their staff. Also, I am thankful for Dr. Deepa Devarajan and the Ess group for all of their help, friendship, and support. Finally, I would like to express my gratitude my family for their love and support. I am grateful for the encouragement I have received from my parents (Charley and Sandy Gustafson), my brothers (Nick Gustafson and Lester Gustafson), my grandparents (Nick and Betty Ferrero), and my sister-in-law (Adrienne Gustafson). I am also extremely thankful for my husband Ben Warner for the time he has given to assist me in raising our son so that I could finish the work presented. I am grateful to for my son Benson and the love and joy he brings me everyday.

Parts of Chapters 3 and 4 were previously published as http://pubs.acs.org/doi/abs/10.1021/acs.organomet.5b00849.

TABLE OF CONTENTS

ABSTRACT ii

ACKNOWLEDGEMENTS iii

TABLE OF CONTENTS iv

LIST OF FIGURES vi

LIST OF TABLES vii

LIST OF SCHEMES viii

1 Introduction 1

1.1 C–H Activation 1

1.2 Brief Overview of Some Transition Metal Catalyzed C–H Activation Reactions 2

1.3 References 5

2 Computational Methods 8

2.2 Specific Computational Methods 10

2.3 DFT Comparison to Experiment 11

2.4 Comparison of DFT Methods to CCSD(t) 13

2.5 Conclusions 14

2.6 References 14

3 Light Alkane C–H Functionalization by Tl(III) 17

3.1 Introduction 17

3.2 $Tl^{III}(TFA)_3$ Model 18

3.3 C–H Activation 20

3.4 M–R Functionalization Mechanisms 26

3.5 Ethylene Bistrifluoroaceticacid Formation 29

3.6 Conclusion 31

3.7 References 31

4 Comparison of Tl^{III} to Hg^{II} and IR^{III} for Reactivity and Partial Oxidation Selectivity for Alkane C–H Functionalization 35

4.1 Introduction 35

4.2 Qualitative Reactivity of Tl^{III} 36

4.3 Comparison of Tl^{III} versus Ir^{III} C–H Activation 40

4.4 Comparison of Tl^{III} to Hg^{II} 43

4.5 Conclusion 47

4.6 References 48

5 Tl^{III}–Alkyl Reductive Functionalization in Water 51

5.1 Introduction 51

5.2 $(OAc)Tl^{III}(CH_3)_2$ Structure 53

5.3 Mechanism for Methyl Group Transfer from $(OAc)Tl^{III}(CH_3)_2$ to $Tl^{III}(OAc)_3$ .. 54

5.4 Functionalization of $(OAc)_2Tl^{III}(CH_3)$ 60

5.5 Conclusion 65

5.6 References 65

LIST OF FIGURES

Figure 3-1. Optimized $Tl^{III}(TFA)_3$ complex featuring three κ^2 TFA ligands with bond lengths varying between 2.34 and 2.36 Å. 19
Figure 3-2. Model structure of the Alkane Complex. (Å) 24
Figure 3-3. TS-1 C–H activation transition state. (Å) 25
Figure 3-4. M–R functionalization transition states. (Å) 28
Figure 4-1. HOMO and LUMO orbitals for $Tl^{III}(TFA)_3$. 37
Figure 4-2. Tl^{III} frontier orbital interactions involved in C–H activation. 38
Figure 4-3. Geometries for the C–H activation and functionalization geometries of Ir^{III} and Tl^{III}. (M = Tl^{III} or Ir^{III}) 41
Figure 4-4. Hg^{II} ground state and methane C–H activation transition state. (Å) 43
Figure 4-5. Gas phase and solvent optimized C–H activation transition state structures. (Å) 46
Figure 5-1. Concerted transition state for methyl and acetate ligand exchange between $(OAc)Tl^{III}(CH_3)_2$ and $Tl^{III}(OAc)_3$. (Å) 60
Figure 5-2. S_N2 M–R functionalization transition states. (kcal/mol) 64

LIST OF TABLES

Table 2-1. Comparison of methods and basis sets for gas phase atomic ionization energies using (U)M06. (eV) 11
Table 2-2. Unrestricted M06 bond dissociation energies. (Zero-point enery corrected values kcal/mol)..... 12
Table 2-3. CCSD(t) and M06 comparison. 13
Table 4-1. M–CH_3 and M–TFA bond dissociation enthalpies for $Tl^{III}(TFA)_3$, $Hg^{II}(TFA)_2$ $(TFA)Hg^{II}–CH_3$ and $(TFA)_2Tl^{III}–CH_3$ in TFAH solvent..... 44
Table 4-2. ΔG_{Solv} values for $Hg^{II}(TFA)_2$ and the C–H activation transition state for $Hg^{II}(TFA)_2$ with methane. (kcal/mol)..... 44
Table 4-3. ΔG_{Solv} values for $Tl^{III}(TFA)_3$ and the C–H activation transition state for $Tl^{III}(TFA)_3$ with methane. (kcal/mol)..... 46
Table 5-1. Homolytic and heterolytic bond energies for $(OAc)Tl^{III}(CH_3)_2$ and the $[Tl^{III}(CH_3)_2]^+$ cation. (kcal/mol; X=OAc)..... 55
Table 5-2. Energetics for open-shell pathways. (kcal/mol) 57
Table 5-3. Energetics for proton transfer from the Dialkylthallium to $Tl^{III}(OAc)_3$. (kcal/mol) ... 57
Table 5-4. Homolytic and heterolytic bond energies of $(OAc)_2Tl^{III}(CH_3)$. (kcal/mol; X= OAc). 61

LIST OF SCHEMES

Scheme 1-1. Outline of C–H activation and M–R functionalization. 1
Scheme 1-2. Two mechanisms for C–H activation. (M = Metal, R = Alkyl group, X = Anionic ligand) 2
Scheme 1-3. Generally accepted Shilov catalytic cycle. 3
Scheme 1-4. Generalized catalytic cycle for Pt^{II} catalyzed oxidation of methane in sulfuric acid. 4
Scheme 1-5. Strassner's proposed catalytic cycle for methane oxidation by $(NHC)Pd(Br)_2$. 4
Scheme 1-6. Ir^{III} oxidation of methane. 5
Scheme 2-1. Model reactions for the Tl^{III} coordination. 13
Scheme 3-1. Tl^{III} oxidation of methane and ethane. 17
Scheme 3-2. Neutral $Tl^{III}(TFA)_3$ model. 19
Scheme 3-3. Ground state cationic $[Tl^{III}(TFA)_2(TFAH)]^+$ model. 20
Scheme 3-4. Open-shell pathways. 21
Scheme 3-5. Additional open-shell pathways examined for the reaction of $Tl^{III}(TFA)_3$ and ethane. 22
Scheme 3-6. Closed-shell pathways for the reaction of $Tl^{III}(TFA)_3$ and Ethane. 22
Scheme 3-7. TS-Hydride 23
Scheme 3-9. Solvent proton shuttling C–H activation transition state. 26
Scheme 3-10. Open-shell M–R functionalization pathway examined. 26
Scheme 3-11. Closed-shell M–R functionalization pathways examined. 27
Scheme 3-12. Outline of ethylene oxidation mechanism. (kcal/mol) 30
Scheme 4-1. Qualitative C–H activation and functionalization energy landscape for oxidation of ethane by $Tl^{III}(TFA)_3$. 37
Scheme 4-2. Qualitative transition-state reactivity model. 39
Scheme 4-3. Comparison of energy landscapes for Tl^{III} and Ir^{III} C–H activation and functionalization with ethane. 42
Scheme 5-1. Proposed reaction pathway for M–R functionalization of $(OAc)Tl^{III}(CH_3)_2$ with $Tl^{III}(OAc)_3$ in water. 52
Scheme 5-2. Mononuclear and dinuclear $(OAc)Tl^{III}(CH_3)_2$ structures examined. 53
Scheme 5-3. Energies for formation of $[Tl^{III}(CH_3)_2]^+$. 54
Scheme 5-4. Possible reductive elimination and M–R functionalization transition states. 56

Scheme 5-5. Methyl transfer pathways from $(OAc)Tl^{III}(CH_3)_2$ to $Tl^{III}(OAc)_3$. (kcal/mol) 58
Scheme 5-6. Methyl transfer pathways from $[Tl^{III}(CH_3)_2]^+$ to $Tl^{III}(OAc)_3$. (kcal/mol) 58
Scheme 5-7. Methyl transfer featuring simultaneous ligand transfer between neutral and cationic thallium dialkyl complex and $Tl^{III}(OAc)_3$. (kcal/mol)..... 59
Scheme 5-8. Functionalization pathways of $(OAc)_2Tl^{III}(CH_3)$. 61
Scheme 5-9. Dissociation of acetate anion. (kcal/mol)..... 62
Scheme 5-10. Nucleophilic attack with water to the Tl^{III}–C bond of the neutral monoalkylthallium complex. (kcal/mol) 63
Scheme 5-11. Methyl dissociation from $[(OAc)Tl^{III}(CH_3)]^+$ with and without explicit solvent. (kcal/mol) 65

1 INTRODUCTION

1.1 C–H Activation

Natural gas is principally methane, but also contains ethane and propane. Light alkanes can be upgraded to larger alkanes or alcohols by steam reforming via synthesis gas,[1] but this process generally requires high temperatures (> 300 °C) and is capital intensive.[2,3] A significant challenge is the direct C–H functionalization of light alkanes to alcohols at temperatures below 200 °C. However, strong C–H bonds, large ionization potentials, and low acidity make light alkanes kinetically difficult to functionalize without significant overoxidation (e.g. to CO_2).[4-6]

Scheme 1-1. Outline of C–H activation and M–R functionalization.

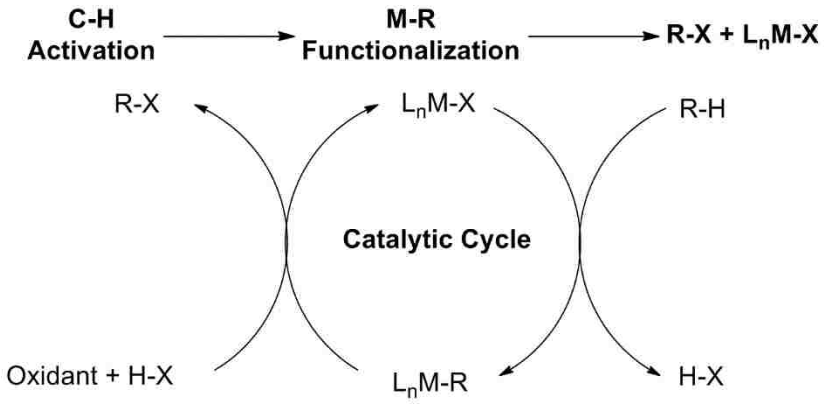

C–H activation is a promising strategy for the direct C–H functionalization of light alkanes.[7-9] C–H activation involves the reaction between a metal–ligand (M–X) complex and

alkane (R–H) to form a metal–alkyl (M–R) intermediate. This "activates" the C–H bond because presumably the M–R intermediate has a weaker bond or is more reactive than the alkane. After C–H activation, subsequent M–R functionalization leads to an upgraded product. Catalysis is achieved by coupling these reactions to catalyst oxidation/regeneration (Scheme 1-1).

There are several possible mechanisms for C–H activation after the alkane C–H bond is weakly coordinated to a metal center. The two extreme mechanisms for generating an M–R intermediate is oxidative addition and σ-bond metathesis/electrophilic substitution (Scheme 1-2).[4,6,8-10] Oxidative addition involves insertion of a metal atom into the C–H bond to make a metal-alkyl hydride. Electrophilic σ-bond metathesis involves forming the metal–alkyl bond with simultaneous transfer of the proton to a ligand.[11] In most cases C–H activation is electrophilic and the metal–alkyl bond formation is more energetically important than the proton transfer.

Scheme 1-2. Two mechanisms for C–H activation. (M = Metal, R = Alkyl group, X = Anionic ligand)

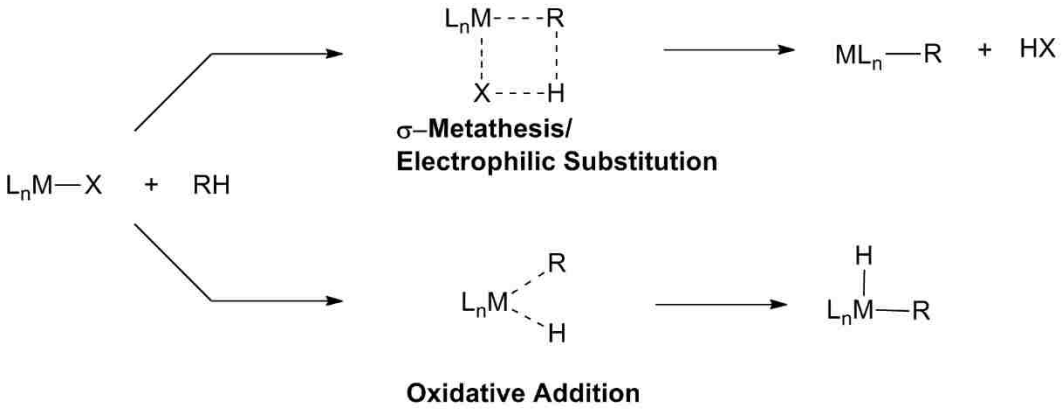

1.2 Brief Overview of Some Transition Metal Catalyzed C–H Activation Reactions

1.2.1 Electrophilic Shilov and Periana C–H Activation

Shilov reported alkane C–H functionalization with catalytic $Pt^{II}Cl_4^{-2}$ in aqueous solvent and stoichiometric $Pt^{IV}Cl_6^{-2}$ as the oxidant (Scheme 1-3).[12-14] The drawbacks of this reaction are stoichiometric Pt^{IV}, low catalyst solubility, and relatively low reactivity.[6] However, this reaction

provided critical inspiration for several catalyst designs. The generally accepted mechanism based on experimental and computational studies involves C–H activation by Pt^{II} to generate a Pt^{II}–alkyl intermediate. Inorganic Pt^{IV} then induces Pt^{II}–alkyl oxidation to Pt^{IV}–alkyl. Water (and chloride) subsequently stimulates M–R functionalization to give a mixture of alcohol and haloalkanes.[12,15]

Scheme 1-3. Generally accepted Shilov catalytic cycle.[12,15]

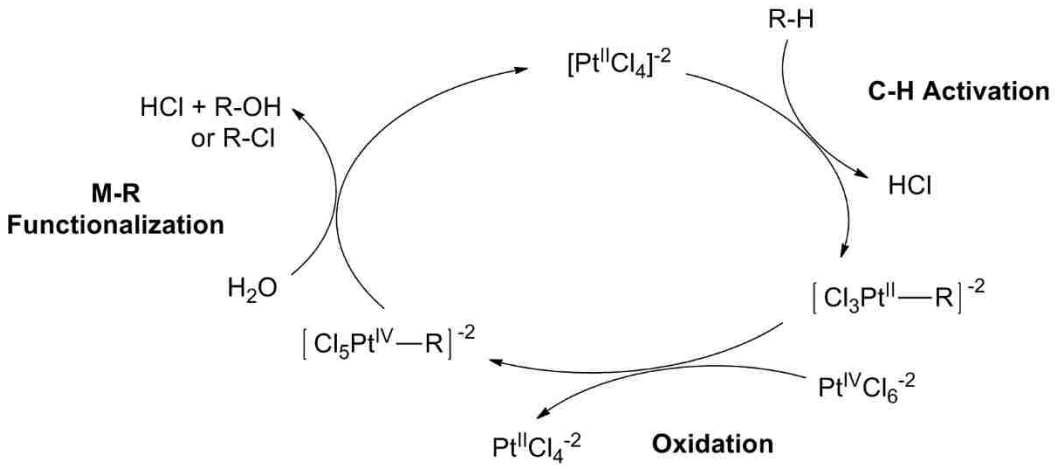

A significant advance in Pt^{II} catalytic electrophilic C–H functionalization of methane was made by Periana at Catalytic Inc. by using a bipyrimidine (bpym) ligand in combination with concentrated sulfuric acid (H_2SO_4) as the solvent and oxidant.[16] Sulfuric acid also decreases the rate of overoxidation that has been termed "product protection". The bpym ligand increases the solubility of the Pt^{II} catalyst and with added SO_3 can result in a product yield up to ~80% and selectivity up to ~90% (versus overoxidation). Based on experimental and computational studies it is proposed that H_2SO_4 facilitates methane coordination to $[(bpym)Pt^{II}(Cl)(HSO_4)]^+$ and then C–H activation occurs by oxidative addition (Scheme 1-4). After deprotonation of the Pt–H bond, SO_3 induces Pt^{II} to Pt^{IV} oxidation and M–R functionalization to form methyl bisulfate (CH_3–OSO_3H).[16,17]

Scheme 1-4. Generalized catalytic cycle for Pt^{II} catalyzed oxidation of methane in sulfuric acid.[16]

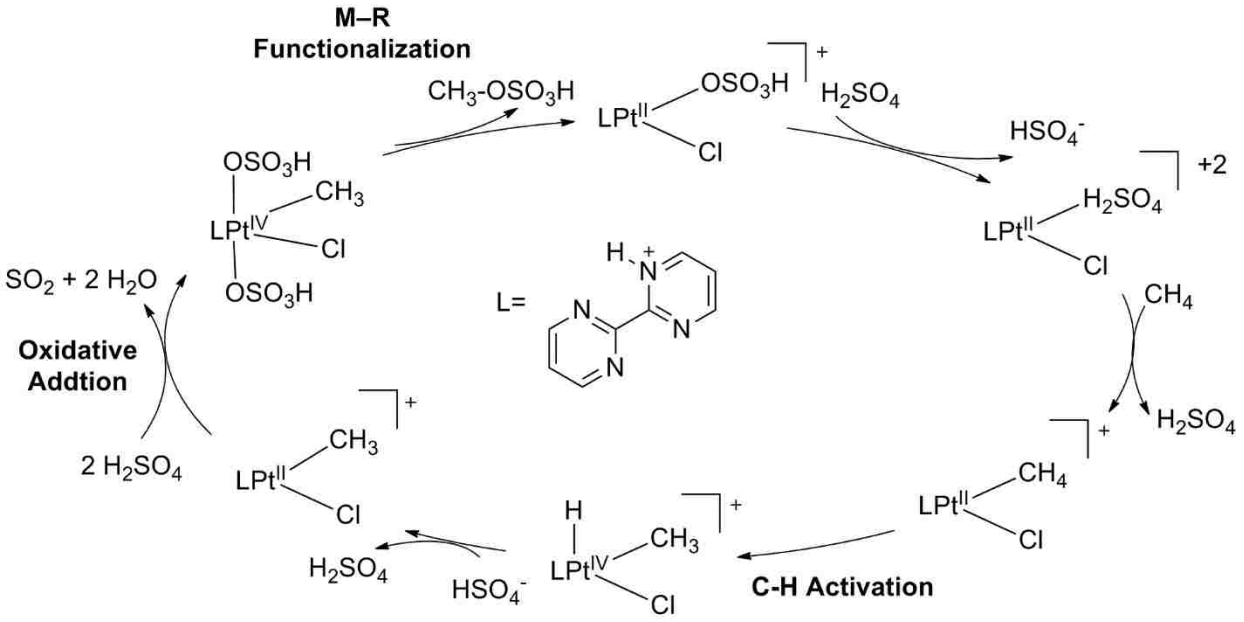

1.2.2 Palladium C–H activation reactions of methane

Scheme 1-5. Strassner's proposed catalytic cycle for methane oxidation by $(NHC)Pd(Br)_2$.[21]

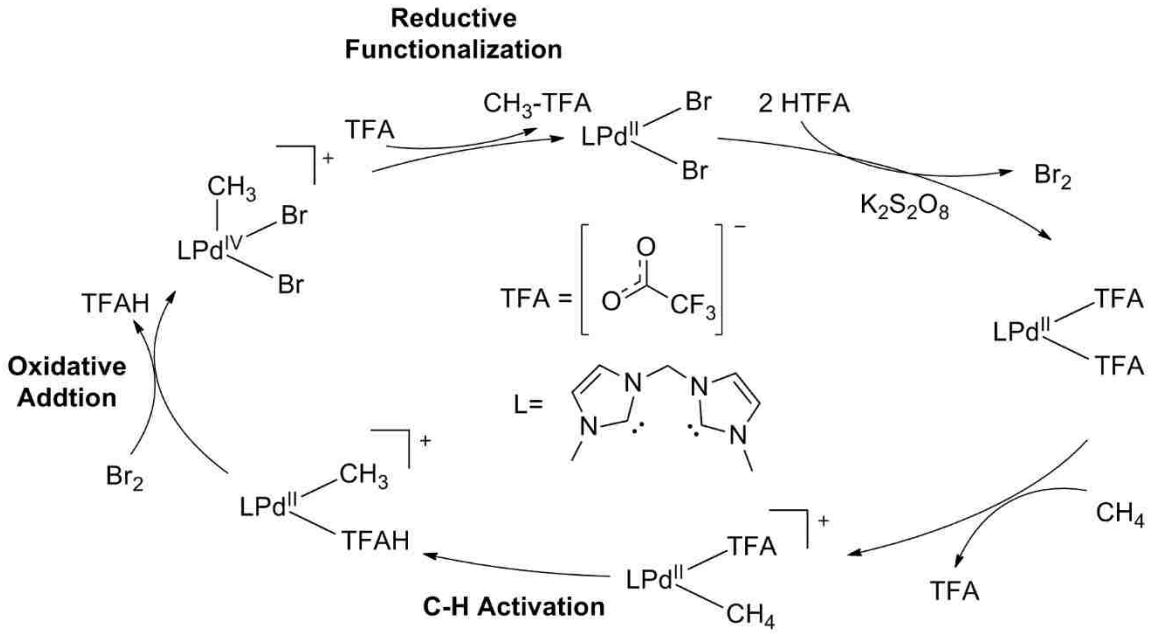

There are also several experimental studies demonstrating Pd-catalyzed C–H activation of alkanes. For example, Pd catalyzes conversion of methane to acetic acid in H_2SO_4[17-19] and Sen and coworkers demonstrated that $Pd^{II}(OAc)_2$ catalytically oxidizes alkanes to alkyltrifluoroacetates in trifluoroacetic acid solvent.[20] Furthermore, Strassner reported that carbene-ligated $Pd^{II}Br_2$ catalysts also oxidize alkanes to alkyltrifluoroacetates (Scheme 1-5) using $K_2S_2O_8$.[21] Based on experiment and computations,[21-28] it is generally proposed that $(NHC)Pd^{II}(TFA)_2$ induces C–H activation by electrophilic substitution. The resulting Pd^{II}–CH_3 complex is oxidized to Pd^{IV} and then functionalized to methyltrifluoroacetate (MeTFA).[23]

1.2.3 Iridium C-H Activation Reactions with Methane

Ir^{III} can also facilitate electrophilic C–H activation to functionalize methane. For example, an Ir^{III}(NNC) (NNC = η^3-6-phenyl-2,2'-bipyridine) complex converts methane to MeTFA in < 5% yield using $NaIO_4$ or KIO_3 (Scheme 1-6).[29] Experimental and computational studies suggest an electrophilic C–H substitution pathway.[6,29,30]

Scheme 1-6. Ir^{III} oxidation of methane. [29]

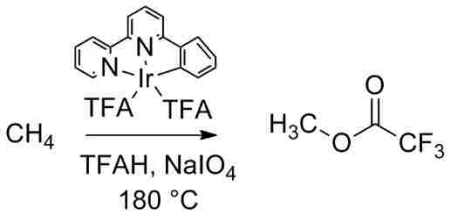

1.3 References

(1) Olah, G. A.; Molnar, A. *Hydrocarbon Chemistry*; 2nd ed.; John Wiley & Sons, Inc.: Hoboken, New Jersey, 2003.

(2) Crabtree, R. H. *Chem. Rev.* **1995**, *95*, 987.

(3) Periana, R. A.; Taube, D. J.; Evitt, E. R.; Löffler, D. G.; Wentrcek, P. R.; Voss, G.; Masuda, T. *Science* **1993**, *259*, 340.

(4) Arndtsen, B. A.; Bergman, R. G.; Mobley, T. A.; Peterson, T. H. *Acc. Chem. Res.* **1995**, *28*, 154.

(5) Bischof, S. M.; Hashiguchi, B. G.; Konnick, M. M.; Periana, R. A. In *Inventing Reactions*; Gooßen, J. L., Ed.; Springer Berlin Heidelberg: Berlin, Heidelberg, 2013, p 195.

(6) Hashiguchi, B. G.; Bischof, S. M.; Konnick, M. M.; Periana, R. A. *Acc. Chem. Res.* **2012**, *45*, 885.

(7) Olah, G. A. *Acc. Chem. Res.* **1987**, *20*, 422.

(8) Crabtree, R. H. *Angew. Chem. Int. Ed.* **1993**, *32*, 789.

(9) Crabtree, R. H. *J. Chem. Soc., Dalton Trans.* **2001**, 2437.

(10) Balcells, D.; Clot, E.; Eisenstein, O. *Chem. Rev.* **2010**, *110*, 749.

(11) Ess, D. H.; Goddard, W. A.; Periana, R. A. *Organometallics* **2010**, *29*, 6459.

(12) Zhu, H.; Ziegler, T. *J. Organomet. Chem.* **2006**, *691*, 4486.

(13) Gol'dshleger, N. F.; Es'kova, V. V.; Shilov, A. E.; Shteinman, A.A., S. *Russ. J. Phys. Chem.* **1972**, *46*, 785.

(14) Goldman, A. S.; Goldberg, K. I. In *Activation and Functionalization of C-H Bonds*; Goldman, A. S., Goldberg, K. I., Eds.; American Chemical Society: Washington, D.C., 2004; Vol. 885, p 1.

(15) Goldman, A. S.; Goldberg, K. I. In *ACS Symposium Series 885* 2004, p 1.

(16) Periana, R. A.; Taube, D. J.; Gamble, S.; Taube, H.; Satoh, T.; Fujii, H. *Science* **1998**, *280*, 560.

(17) Periana, R. A.; Mironov, O.; Taube, D.; Bhalla, G.; Jones, C. *Science* **2003**, *301*, 814.

(18) Zerella, M.; Kahros, A.; Bell, A. T. *J. Catal.* **2006**, *237*, 111.

(19) Zerella, M.; Mukhopadhyay, S.; Bell, A. T. *Chem. Commun.* **2004**, 1948.

(20) Gretz, E.; Oliver, T. F.; Sen, A. *J. Am. Chem. Soc* **1987**, *109*, 8109.

(21) Munz, D.; Strassner, T. *Top. Catal.* **2014**, *57*, 1372.

(22) Ahrens, S.; Strassner, T. *Inorg. Chim. Acta* **2006**, *359*, 4789.

(23) Ahrens, S.; Zeller, A.; Taige, M.; Strassner, T. *Organometallics* **2006**, *25*, 5409.

(24) Meyer, D.; Taige, M. A.; Zeller, A.; Hohlfeld, K.; Ahrens, S.; Strassner, T. *Organometallics* **2009**, *28*, 2142.

(25) Muehlhofer, M.; Strassner, T.; Herrmann, W. A. *Angew. Chem. Int. Ed.* **2002**, *41*, 1745.

(26) Munz, D.; Meyer, D.; Strassner, T. *Organometallics* **2013**, *32*, 3469.

(27) Munz, D.; Strassner, T. *Chem. -Eur. J.* **2014**, *20*, 14872.

(28) Strassner, T.; Muehlhofer, M.; Zeller, A.; Herdtweck, E.; Herrmann, W. A. *J. Organomet. Chem.* **2004**, *689*, 1418.

(29) Young, K. J. H.; Oxgaard, J.; Ess, D. H.; Meier, S. K.; Stewart, T.; Goddard III, W. A.; Periana, R. A. *Chem. Commun.* **2009**, 3270.

(30) Hashiguchi, B. G.; Hövelmann, C. H.; Bischof, S. M.; Lokare, K. S.; Leung, C. H.; Periana, R. A. In *Encyclopedia of Inorganic Chemistry*; John Wiley & Sons, Ltd: 2006.

2 COMPUTATIONAL METHODS

2.1.1 Density Functional Theory

Density-functional theory (DFT) is a balance of computational cost and accuracy for energies and structures.[1] Therefore, it is the primary computational tool used in this dissertation. DFT is computationally efficient because ground-state energies and molecular properties are calculated using the ground-state electron density, $\rho(r)$, instead of a highly complex wavefunction. However, the exact functional that maps the electron density into energy is unknown. Therefore, over the past several decades a variety of density functionals with varying levels of approximations have been developed and tested.

There are several so-called rungs of DFT functionals.[2] The first rung is the local density approximation (LDA) and local spin density approximation (LSDA). The LDA/LSDA approximation calculates the energy of the exchange correlation directly from $\rho(r)$.[1,3] The second rung of DFT functionals is the so-called generalized gradient approximation (GGA) functionals that takes into account that electron density is not spatially uniform.[4,5] This functional can mimic the correct asymptotic behavior of the energy density.[6] An example of a GGA functional is Becke's B88.[7] The third rung, meta-GGAs, are similar to GGAs but they utilize a second derivative of the electron density (e.g. Becke's B95 correlation functional).[8]

The fourth rung of DFT functionals are hybrid functionals that add a percentange of exact Hartree–Fock (HF) exchange to the functional. For example, the older B3LYP functional uses LSDA, HF, and B88 exchange terms along with VWN and LYP functional correlation terms. There are two common formulations of hybrid functionals, global and range-separated functionals, depending on whether the percentage of HF exchange is constant or varies as a function of distance.[5]

The M06 functional is a hybrid meta-GGA functional and is used extensively in this work. M06 has 27% of exact HF exchange, and includes parameters from the spin density, reduced spin density, and spin kinetic energy density. The M06 functional is recommended for organometallic systems.[9]

2.1.2 Basis Sets

Generally in DFT the density is constructed from Kohn–Sham orbitals with a specific basis set.[6] The Gaussian basis sets used in this work are Cartesian-based functions. The Pople-type basis sets use contracted Gaussian-type orbitals (CGTOs) for core orbitals and Gaussian-type orbitals (GTOs) for valence orbitals.[10-13] One example is the 6-31+G(d,p) basis set.[14,15] This basis set uses six CGTOs for the core electrons, and three CGTOs with one GTO for the valence electrons. The "+" indicates diffuse functions are used for all non-hydrogen atoms and the d and p indicate polarization functions on heavy and hydrogen atoms.[16] The correlation consistent basis sets account for the correlation energy of valence electrons. One example of a correlation consistent basis set is the aug-cc-pVTZ basis set. "Aug" indicates the use of diffuse functions and "pVTZ" refers to a polarized valence triple ζ basis set.[17,18]

For atoms with many electrons it is impractical to use basis functions for all electrons. Furthermore, core electrons of heavy atoms are generally not well modeled by traditional basis

sets due to relativistic effects. Therefore, for transition metals and heavy main-group metals a pseudopotential and basis was used where core electrons are replaced with a pseudopotential that replicates the effects the core electrons have on the valence electrons.[3]

2.2 Specific Computational Methods

Optimized ground-state and transition-state geometries were obtained using the Gaussian 09[19] program with the M06[9] density functional and an ultrafine integration grid. Transition-state and minima structures were confirmed by normal-mode vibrational frequency analysis. All conformations for each structure were extensively searched and only the lowest-energy structures are reported. Optimized structures were obtained with the 6-31+G(d,p)[14,15] basis sets for all atoms except Tl. Structures containing Tl were optimized with the LANL2DZ[20] basis sets. Single point energy corrections were taken with the aug-cc-pVTZ[21-23] basis set for all atoms except Tl. Single point energies for structures with Tl used the CC-pwCVTZ-pp.[21-23] Reported M06/aug-cc-pVTZ[CC-pwCVTZ-pp] enthalpies and Gibbs free energies were calculated with energy corrections from the M06/6-31+G(d,p)[LANL2DZ] optimized energies. In addition, all reported enthalpies and Gibbs free energies include solvation (ΔG_{solv}) corrections. All reported 3D structures were generated with the CYLview[24] program and all schemes were generated with the ChemBioDraw program.[25]

Solvation (ΔG_{solv}) was treated using a continuum solvation model in Gaussian 09. For structures in trifluoroacetic acid (TFAH) the SMD solvent model was used for water with the dielectric changed to 8.42 and solvent radius changed to 2.479 Å.[26] This general procedure has been used in a few previous studies.[27-29]In some cases, explicit TFAH or water was added in addition to the continuum model.

2.3 DFT Comparison to Experiment

While the M06 functional generally performs well for transition metals,[2,30] it was not clear at the onset of this study that it would be accurate for high oxidation state main-group metals. Therefore, the performance of the M06 functional with several basis sets was tested for Hg and Tl. Table 2-1 compares calculated and experimental gas phase atomic ionization energies for Tl cations. Ionization energies for conversion of Tl^{+1} to Tl^{+2} and Tl^{+3} were chosen since these are the oxidation states that are used in the alkane oxidation reactions modeled in this work.(Table 2-1)

Table 2-1. Comparison of methods and basis sets for gas phase atomic ionization energies using (U)M06. (eV)

	LANL2DZ	cc-pwCVDZ	cc-pwCVTZ	def2-TZVPPD	Experiment[31]
$Hg \rightarrow Hg^{+}$	9.36	10.27	10.28	10.28	10.44
$Hg^{+} \rightarrow Hg^{2+}$	16.93	18.62	18.62	18.59	18.76
$Tl^{+} \rightarrow Tl^{2+}$	19.2	20.3	20.34	20.31	20.43
$Tl^{2+} \rightarrow Tl^{3+}$	28.21	29.75	29.73	29.75	29.85

The values in Table 2-1 indicate that for Hg^{0}, Hg^{+1}, Tl^{+1}, and Tl^{+2} atomic ionization energies the LANL2DZ effective core potential and basis set is extremely inadequate with errors exceeding 1 eV. For example, the experimentally measured gas-phase ionization energy for conversion of Tl^{2+} to Tl^{3+} is 29.85 eV. The calculated M06/LANL2DZ value is 28.21 eV, which underestimates the ionization energy by 1.64 eV. Interestingly, the small cc-pwCVDZ effective core potential and basis set show significant improvement over LANL2DZ with errors between 0.1-0.2 eV. The use of a TZ basis set, either cc-pwCVTZ or def2-TZVPPD, did not significantly improve the calculated values compared to experiment.

Even though the choice of effective core potential and basis set plays a critical role for estimating energies, test calculations show that for optimization of geometries there is a small

difference between LANL2DZ and cc-pwCVDZ or def2-TZVPPD basis sets. Therefore, the procedure selected to generate final energies involves optimization with the LANL2DZ basis set for Tl and the 6-31+G(d,p) basis set for all other atoms. This level of theory was used for frequency calculations and thermochemical corrections. Final electronic energies were obtained with the cc-pwCVTZ-pp basis set for Tl and aug-cc-CVTZ basis set for all other atoms.

The accuracy of Hg^{II} and Tl^{III} metal–alkyl (M–R) bond strengths were also examined. Accurate experimental Tl^{III}–C bond strengths are unavailable, but Hg^{II}–C bond strengths are known.[32] Table 2-2 below reports the calculated (U)M06 bond dissociation energies for $Hg^{II}(CH_3)_2$ and $Tl^{III}(CH_3)_3$.

Table 2-2. Unrestricted M06 bond dissociation energies. (Zero-point enery corrected values kcal/mol)

	6-31+G(d,p)/ [LANL2DZ]	aug-cc-pVDZ/ cc-pwCVDZ	aug-cc-pVTZ/ cc-pwCVTZ	def2-TZVPPD	Experiment[32]
$Hg(CH_3)_2 \rightarrow$ $Hg + 2(\bullet CH_3)$	46.5	59.9	58.6	58.8	57.2 ± 1.5
$Hg(CH_3)_2 \rightarrow$ $\bullet HgCH_3 + \bullet CH_3$	43.9	57.1	56.3	55.5	
$Tl(CH_3)_3 \rightarrow$ $\bullet Tl(CH_3)_2 + \bullet CH_3$	50.1	50.9	50.5	51.2	

Similar to the ionization energies, the combination of the 6-31+G(d,p) and LANL2DZ potential and basis set results in a significant error that underestimates Hg–C bond strengths by over 10 kcal/mol. The use of a small effective core potential combined with either a DZ or TZ valence basis set provides Hg–C bond strengths very close to experiment. While the choice of effective core potential and basis set has a significant impact on the prediction of Hg–C bond strengths, there is a much less dramatic impact on the prediction of Tl–C bond strengths. For example, Table 2 reports that all four basis sets examined with the M06 functional predict a very narrow range (< 2 kcal/mol) of Tl–C bond dissociation energies for $Tl(CH_3)_3$.

2.4 Comparison of DFT Methods to CCSD(t)

Scheme 2-1. Model reactions for the Tl^{III} coordination.

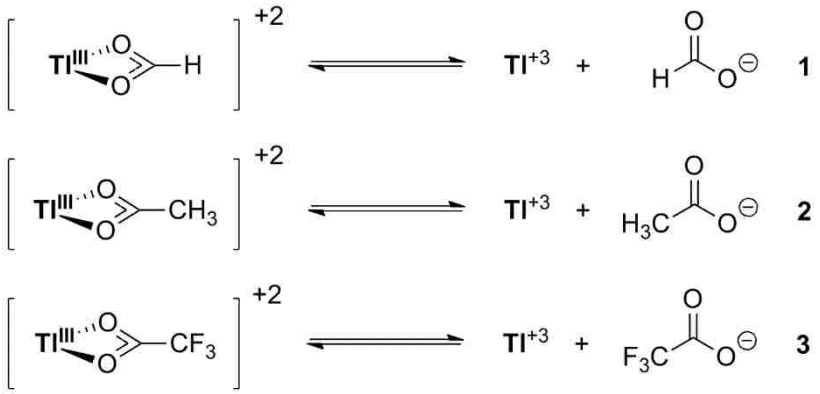

Table 2-3. CCSD(t) and M06 comparison.

	Coordination 1	**Coordination 2**	**Coordination 3**
	Δ*E* (kcal/mol)	Δ*E* (kcal/mol)	Δ*E* (kcal/mol)
M06/cc-pwCVTZ	700.4	722.9	679.4
M06/def2-TZVPPD	701.0	723.3	680.1
	ΔCCSD(t)	ΔCCSD(t)	ΔCCSD(t)
def2-SVP	676.6	700.5	650.9
def2-TZVP	699.5	725.5	676.5
def2-TZVPP	699.1	724.9	
def2-TZVPPD	695.7	722.2	
def2-QZVP	700.6		

CCSD(t) calculations are considered to be experimentally accurate. As another method to test the accuracy of M06 calculations, Table 2-1 compares gas phase CCSD(t) and M06 Tl-anion coordination energies. The def2 basis functions for the CCSD(t) method were increased systematically to show convergence. The structures optimized with the M06 density functional were optimized with the LANL2DZ basis set for thallium and 6-31+G(d,p) for all other atoms. Single point calculations were performed with the cc-pwCVTZ basis set for Tl and with the aug-CC-pVTZ basis set for the remaining atoms. The results in Table 2-3 show a maximum difference

of 5 kcal/mol between the M06 method and CCSD(t) with a small basis set. With a large basis set the difference is ~1 kcal/mol.

2.5 Conclusions

The accuracy of the M06 density functional with the LANL2DZ/6-31+G(d,p) and CC-pwCVTZ-pp/aug-cc-CVTZ basis sets were examined. The LANL2DZ/6-31+G(d,p) basis sets were unable to correctly predict the experimental oxidation potentials. The CC-pwCVTZ-pp/aug-cc-CVTZ basis sets with M06 were able to predict Hg and Tl ionization energies within ~0.2 eV.

2.6 References

(1) Cramer, C. J. *Essentials of Computational Chemistry*; 2 ed.; John Wiley & Sons, Ltd.: Hoboken, NJ, 2004.

(2) Zhao, Y.; Truhlar, D. G. *Acc. Chem. Res.* **2008**, *41*, 157.

(3) Levine, I. N. *Quantum Chemistry*; Pearson Prentice Hall Upper Saddle River, NJ, 2009; Vol. 6.

(4) Kohn, W.; Sham, L. J. *Physical Review* **1965**, *140*, A1133.

(5) Kohn, W.; Sham, L. J. *Physical Review* **1965**, *137*, A1697.

(6) Becke, A. D. *Physical Review A* **1988**, *38*, 3098.

(7) Becke, A. D. *J. Chem. Phys* **1988**, *88*, 1053.

(8) Becke, A. D. *J. Chem. Phys* **1996**, *104*, 1040.

(9) Zhao, Y.; Truhlar, D. G. *Theor. Chem. Acc.* **2008**, *120*, 215.

(10) Hehre, W. J.; Ditchfield, R.; Pople, J. A. *J. Chem. Phys* **1972**, *56*, 2257.

(11) Ditchfield, R.; Hehre, W. J.; Pople, J. A. *J. Chem. Phys* **1971**, *54*, 724.

(12) Rassolov, V. A.; Pople, J. A.; Ratner, M. A.; Windus, T. L. *J. Chem. Phys* **1998**, *109*, 1223.

(13) Rassolov, V. A.; Ratner, M. A.; Pople, J. A.; Redfern, P. C.; Curtiss, L. A. *J. Comput. Chem.* **2001**, *22*, 976.

(14) Petersson, G. A.; Bennett, A.; Tensfeldt, T. G.; Al-Laham, M. A.; Shirley, W. A.; Mantzaris, J. *J. Chem. Phys* **1988**, *89*, 2193.

(15) Petersson, G. A.; Al-Laham, M. A. *J. Chem. Phys* **1991**, *94*, 6081.

(16) Hariharan, P. C.; Pople, J. A. *Theoretica chimica acta* **1973**, *28*, 213.

(17) Pople, J. A.; Head-Gordon, M.; Raghavachari, K. *J. Chem. Phys* **1987**, *87*, 5968.

(18) Pople, J. A.; Krishnan, R.; Schlegel, H. B.; Binkley, J. S. *International Journal of Quantum Chemistry* **1978**, *14*, 545.

(19) Frisch, M. J.; Trucks, G. W.; Schlegel, H. B.; Scuseria, G. E.; Robb, M. A.; Cheeseman, J. R.; Scalmani, G.; Barone, V.; Mennucci, B.; Petersson, G. A.; Nakatsuji, H.; Caricato, M.; Li, X.; Hratchian, H. P.; Izmaylov, A. F.; Bloino, J.; Zheng, G.; Sonnenberg, J. L.; Hada, M.; Ehara, M.; Toyota, K.; Fukuda, R.; Hasegawa, J.; Ishida, M.; Nakajima, T.; Honda, Y.; Kitao, O.; Nakai, H.; Vreven, T.; Montgomery Jr., J. A.; Peralta, J. E.; Ogliaro, F.; Bearpark, M. J.; Heyd, J.; Brothers, E. N.; Kudin, K. N.; Staroverov, V. N.; Kobayashi, R.; Normand, J.; Raghavachari, K.; Rendell, A. P.; Burant, J. C.; Iyengar, S. S.; Tomasi, J.; Cossi, M.; Rega, N.; Millam, N. J.; Klene, M.; Knox, J. E.; Cross, J. B.; Bakken, V.; Adamo, C.; Jaramillo, J.; Gomperts, R.; Stratmann, R. E.; Yazyev, O.; Austin, A. J.; Cammi, R.; Pomelli, C.; Ochterski, J. W.; Martin, R. L.; Morokuma, K.; Zakrzewski, V. G.; Voth, G. A.; Salvador, P.; Dannenberg, J. J.; Dapprich, S.; Daniels, A. D.; Farkas, Ö.; Foresman, J. B.; Ortiz, J. V.; Cioslowski, J.; Fox, D. J. Gaussian, Inc.: Wallingford, CT, USA, 2009.

(20) Wadt, W. R.; Hay, P. J. *J. Chem. Phys* **1985**, *82*, 284.

(21) Peterson, K. A.; Puzzarini, C. *Theor. Chem. Acc.* **2005**, *114*, 283.

(22) Figgen, D.; Rauhut, G.; Dolg, M.; Stoll, H. *Chem. Phys.* **2005**, *311*, 227.

(23) This basis set was downloaded from https://bse.pnl.gov/bse/portal.

(24) Legault, C. Y.; Université de Sherbrooke: 2009. (http://www.cylview.org).

(25) In *ChemBioDraw*; 12.0.2.1076 ed.; CambridgeSoft: 2010, p 13649.

(26) Marenich, A. V.; Cramer, C. J.; Truhlar, D. G. *J. Phys. Chem. B* **2009**, *113*, 6378.

(27) Butler, R. N. *Chem. Rev.* **1984**, *84*, 249.

(28) Lau, W.; Huffman, J. C.; Kochi, J. K. *J. Am. Chem. Soc* **1982**, *104*, 5515.

(29) Hashiguchi, B. G.; Konnick, M. M.; Bischof, S. M.; Gustafson, S. J.; Devarajan, D.; Gunsalus, N.; Ess, D. H.; Periana, R. A. *Science* **2014**, *343*, 1232.

(30) Zhao, Y.; Truhlar, D. G. *J. Chem. Phys* **2006**, *124*, 224105.

(31) NIST Atomic Spectra Database (ver. 5.2), http://physics.nist.gov/asd.

(32) Carson, A. S.; Carson, E. M.; Wilmshurst, B. *Nature* **1952**, *170*, 320.

3 LIGHT ALKANE C–H FUNCTIONALIZATION BY TL(III)

3.1 Introduction

C–H oxygen functionalization of alkanes can be promoted by a variety of transition metals such as Pt,[1-4] Pd,[5-13] Rh,[14-20] and Ir.[21-40] Main-group metals can also promote alkane C–H functionalization. For example, $Tl^{III}(TFA)_3$ (TFA = trifluoroacetate) oxidizes methane and ethane in trifluoroacetic acid (TFAH) to their corresponding trifluoroacetate esters with a small amount of carbon over-oxidation (Scheme 3-1).[41] For ethane, oxidation results in an approximately 2:1 mixture of ethyl trifluoroacetate (EtTFA) to ethane-1,2-diyl bis(2,2,2-trifluoroacetate) ($EG(TFA)_2$).

Scheme 3-1. Tl^{III} oxidation of methane and ethane.[41]

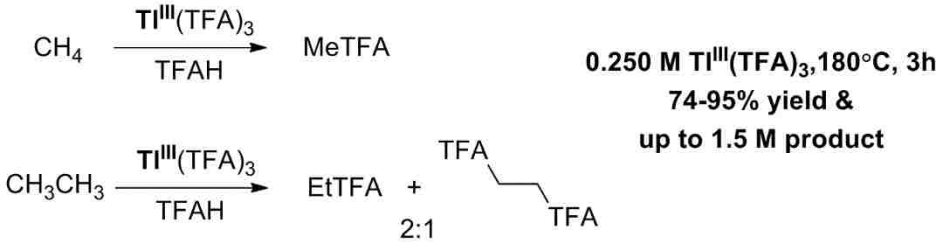

$Tl^{III}(TFA)_3$ oxidation of hydrocarbon C–H bonds is not new. Kochi[42-44] and others[45-47] have reported arene C–H bond oxidation by $Tl^{III}(TFA)_3$ in TFAH solvent. Arene C–H oxidation is proposed to occur by an electrophilic aromatic substitution mechanism and ESR studies have detected electron transfer (ET) intermediates.[42-44] Alkane oxidation by $Tl^{III}(TFA)_3$ is surprising

because the relatively similar $Hg^{II}(TFA)_2$, which has the same d^{10} electronic configuration, does not induce C–H oxidation.[41,48]

This chapter reports density-functional theory (DFT) calculations that demonstrate that $Tl^{III}(TFA)_3$ oxidizes alkanes by a C–H activation mechanism and the corresponding metal–alkyl (M–R) intermediate undergoes closed-shell functionalization. The use of high-oxidation state main-group metals to promote both C–H activation and M–R functionalization represents a new strategy for alkane partial oxidation. Calculations indicate that the unique feature of p-block main-group metals, such as Tl^{III}, versus d-block metals is the very fast M–R functionalization step.

3.2 $Tl^{III}(TFA)_3$ Model

Figure 3-1 displays the optimized ground-state structure of $Tl^{III}(TFA)_3$. There are several low-energy TFA ligand coordination geometries. The lowest energy structure identified involves three bidentate TFA ligands coordinated to its metal center in a κ^2 fashion. The lowest energy spin state for this d^{10} $Tl^{III}(TFA)_3$ complex is a singlet. Triplet and quintet spin states are 54.4 and 147.0 kcal/mol higher in enthalpy than the singlet ground state.

$Tl^{III}(TFA)_3$ can also be modeled with explicit TFAH solvent molecules coordinated to the metal center to give $Tl^{III}(TFA)_3(TFAH)_n$ type complexes where n = 1-3. (Scheme 3-2a) Coordination of an explicit TFAH solvent requires a κ^2 trifluoroacetate ligand to convert to a κ^1 interaction and ΔH = –13.7 and ΔG = –0.5 kcal/mol for coordination. This suggests that solvent coordination and an associative exchange will facilitate rapid exchange of TFA ligands and indicates that these compounds are likely in equilibrium. These energetics are not definitive and suggest inner-sphere solvent coordination. Therefore, the κ^2 $Tl^{III}(TFA)_3$ model is used since it corresponds to the experimental X-ray structure.[49,50]

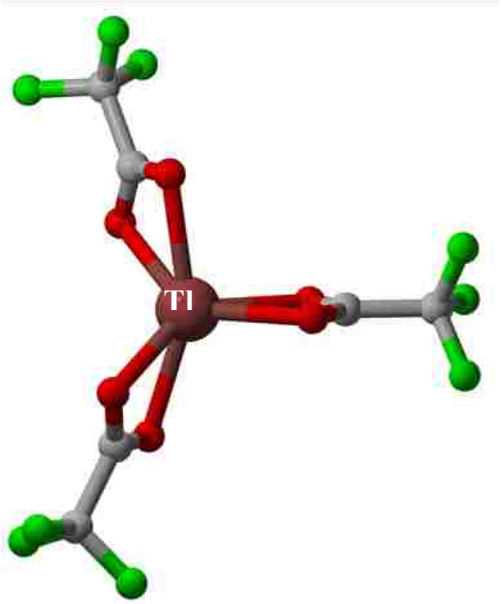

Figure 3-1. Optimized $Tl^{III}(TFA)_3$ complex featuring three κ^2 TFA ligands with bond lengths varying between 2.34 and 2.36 Å.

Scheme 3-2. Neutral $Tl^{III}(TFA)_3$ model.

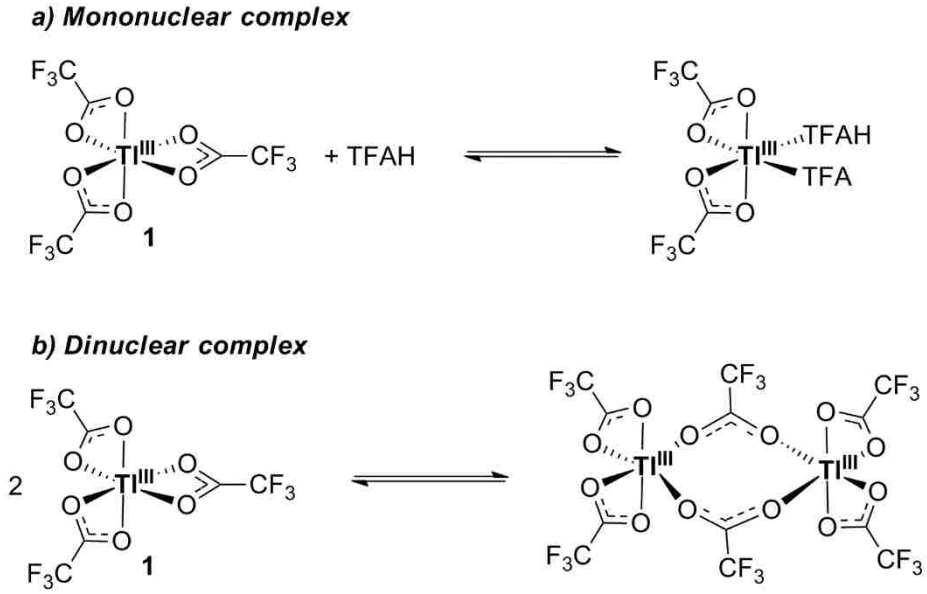

A polynuclear d^{10} metal TFA π complex[51] observed by Lau et al. prompted examination of dinuclear $Tl^{III}_2(TFA)_6$ complexes such as the one shown in Scheme 3-2b. However, comparison calculations suggest that $Tl^{III}_2(TFA)_6$ result in activation barriers that are quite similar to $Tl^{III}(TFA)_3$. Also, arene and cyclopropane oxidation kinetic studies with $Tl^{III}(TFA)_3$ have a first-

order rate dependence on Tl^{III}.[52-54] Therefore, a dinuclear model does not provide a significant advantage over a mononuclear model.

Conversion of one κ^2 carboxylate interaction into a κ^1 carboxylate interaction on $Tl^{III}(TFA)_3$ requires $\Delta H = 9.4$ kcal/mol to create a "vacant" coordination site. Complete TFA ligand dissociation to form the monocation $[Tl^{III}(TFA)_2]^+$ requires $\Delta H = 38.7$ and $\Delta G = 40.3$ kcal/mol. Comparison of M06/cc-pwCVDZ-pp to CCSD(T)/cc-pVTZ energies show a difference of no more than 1 kcal/mol (see Chapter 2). Scheme 3-3 shows the estimate for forming the monocationic species with explicit TFAH solvent. The calculated ΔH and ΔG for this equilibrium is 24.5 and 38.0 kcal/mol. These energetics disfavor a monocationic species, but do not rule them out for kinetic pathways; therefore, reaction mechanisms were explored with both $Tl^{III}(TFA)_3$ and $[Tl^{III}(TFA)_2]^+$.

Scheme 3-3. Ground state cationic $[Tl^{III}(TFA)_2(TFAH)]^+$ model.

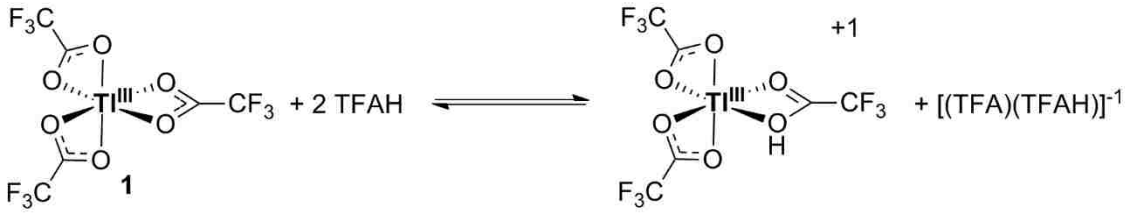

3.3 C–H Activation

3.3.1 Open-shell pathways

While Tl^{III} complexes are generally overall two-electron oxidants, the large reduction potential suggests that a Tl^{III} complex could act as a one-electron oxidant towards alkanes.[55] Additionally, Kochi observed radical cation intermediates during arene C–H bond oxidation with $Tl^{III}(TFA)_3$.[43,44,51] Thus, multiple open-shell pathways for reaction between $Tl^{III}(TFA)_3$ and ethane were examined.

Scheme 3-4 depicts initiation of open-shell pathways through Tl^{III}–O bond homolysis to create the $[Tl^{III}(TFA)_2]^{\bullet}$ and $[CF_3COO]^{\bullet}$ radical pair and ET to generate the $[Tl^{III}(TFA)_3]^{\bullet-}$ radical anion and ethyl radical cation.

Scheme 3-4. Open-shell pathways.

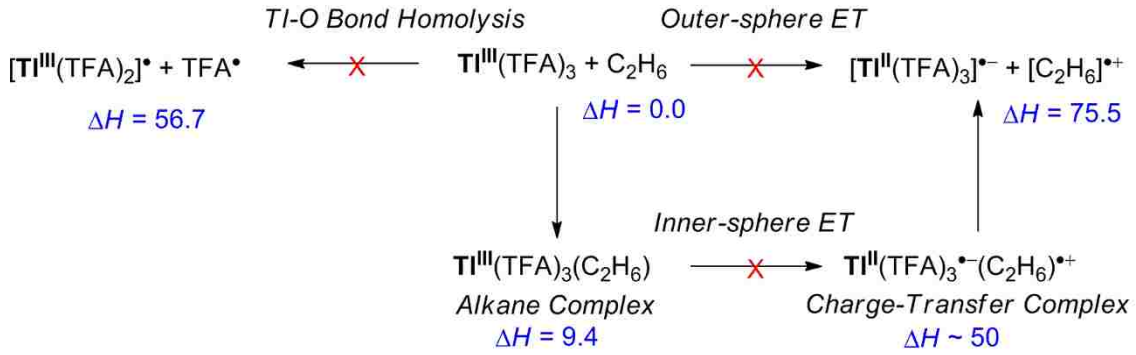

The relatively large Tl^{III}–O bond homolysis enthalpy of 56.7 kcal/mol indicates that forming the Tl^{II} and TFA radicals is unlikely. Outer-sphere ET from ethane to Tl^{III} requires 75.5 kcal/mol. Inner-sphere ET is possible from a $Tl^{III}(TFA)_3$–ethane coordination complex, similar to the charge-transfer complex proposed by Kochi for Tl^{III} and arenes.[42,43,51] Accurate inner-sphere ET energies are difficult to estimate. A TD-DFT estimate of charge transfer suggests this requires over ~50 kcal/mol. This is consistent with the ESR studies where ET only occurs with electron-rich arenes, such as pentamethylbenzene.[43,44,51]The prediction of highly endothermic ET thermodynamics is also consistent with very little C–C bond fragmentation of ethane during oxidation by $Tl^{III}(TFA)_3$.

Scheme 3-5 shows three other open-shell pathways examined. Even though $Tl^{III}(TFA)_2^+$ is a more potent electron acceptor compared to neutral Tl^{III}, the ΔH for outer-sphere ET between $Tl^{III}(TFA)_2^+$ and ethane is 43.4 kcal/mol. Again, this suggests that electron oxidation pathways are not viable. Alternative to ET, proton-coupled electron transfer (PCET) leads to the $[Tl^{II}(TFA)_2(TFAH)]^{\bullet}$ complex and ethyl radical. In this pathway the electron from ethane is

transferred to the Tl^{III} metal center and the proton is transferred to a TFA ligand. With ΔH = 27.4 kcal/mol this process is significantly more favorable than outer-sphere or inner-sphere ET. Much less favorable is the hydrogen atom transfer (Scheme 3-5c) to give a Tl^{III}–H. This pathway has a large thermodynamic penalty of ΔH = 100.5 kcal/mol due to the use of a core 5d electron.

Scheme 3-5. Additional open-shell pathways examined for the reaction of $Tl^{III}(TFA)_3$ and ethane.

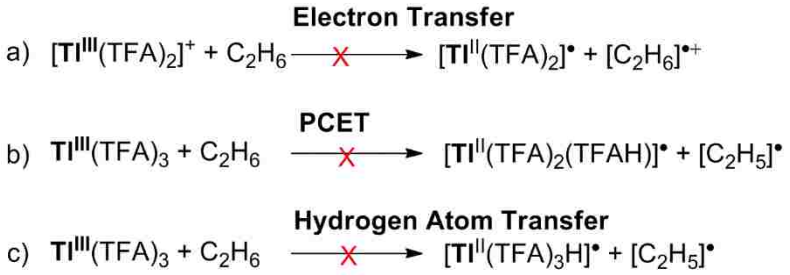

3.3.2 Closed-shell pathways

Hydride transfer (Scheme 3-6A) from ethane to $Tl^{III}(TFA)_3$ to give the ethyl cation and $[Tl^{III}(TFA)_3(H)]^-$ requires ΔH = 45.4 kcal/mol. Hydride transfer to $Tl^{III}(TFA)_2^+$ is thermodynamically favorable with ΔH of –10.7 kcal/mol and the hydride abstraction transition state has an activation enthalpy of 17.7 kcal/mol (Scheme 3-7). The Tl^{III} monocation is ~24 kcal/mol endothermic and combined with the barrier height for hydride transfer suggests this pathway requires > 40 kcal/mol.

Scheme 3-6. Closed-shell pathways for the reaction of $Tl^{III}(TFA)_3$ and Ethane.

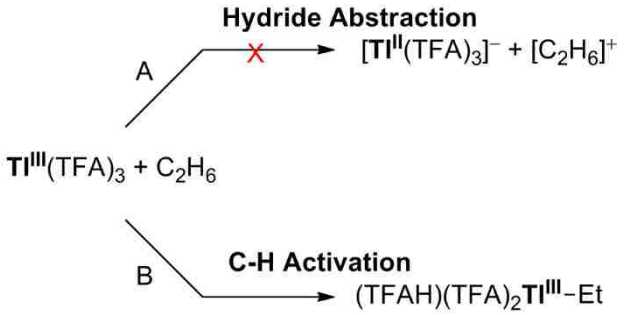

Scheme 3-7. TS-Hydride

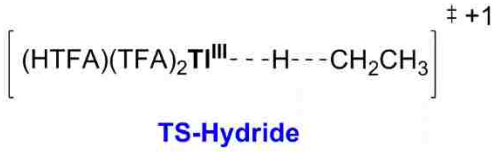

TS-Hydride

The C–H activation reaction (Scheme 3-8) between $Tl^{III}(TFA)_3$ and ethane leads to a Tl^{III}–CH_2CH_3 intermediate. The Tl^{III}–CH_2CH_3 intermediate is exothermic by 23.6 kcal/mol. The kinetic pathway potentially involves the formation of an ethane coordination complex $(TFA)_3Tl^{III}(C_2H_6)$ (Figure 3-2) with ΔH = 9.4 kcal/mol. The C–H bond cleavage transition state forms a Tl^{III}–C bond with simultaneous C–H bond deprotonation by a TFA ligand. This structure is similar to previously reported metal-acetate transition states for C–H activation. The intrinsic reaction coordinate (IRC) of the C–H activation transition state indicates that the ethane complex does not proceed by the C–H activation transition state. The $\Delta H^{‡}$ for TS-1 is 19.6 kcal/mol and is lower in enthalpy than all other open-shell pathways examined and hydride abstraction.

The IRC of TS-1 directly connects the $(TFA)_2(TFAH)Tl^{III}$–CH_2CH_3 intermediate with the ground-state structure of $Tl^{III}(TFA)_3$ and dissociated ethane. Because the IRC directly connects the reactants and the intermediate, this indicates that a TFA ligand does not completely dissociate from $Tl^{III}(TFA)_3$ to form the cationic $Tl^{III}(TFA)_2^+$ complex prior to TS-1. This is consistent with the calculated TFA ligand dissociation values as discussed in Section 3.2 where TFA dissociation requires at least ΔH = 24.5 kcal/mol.

The calculated kinetic isotope effect (KIE) further supports the C–H activation transition-state model (Figure 3-3). The KIE for CH_3CD_3 C–H/C–D activation was estimated using only a difference of transition-state zero-point energies and resulted in a value of 4.7, which is close to the experimental value of 3.8. Estimation of the KIE based on the differences in free energy results in a value of 5.8.

Scheme 3-8. Neutral vs cationic C–H activation pathways.

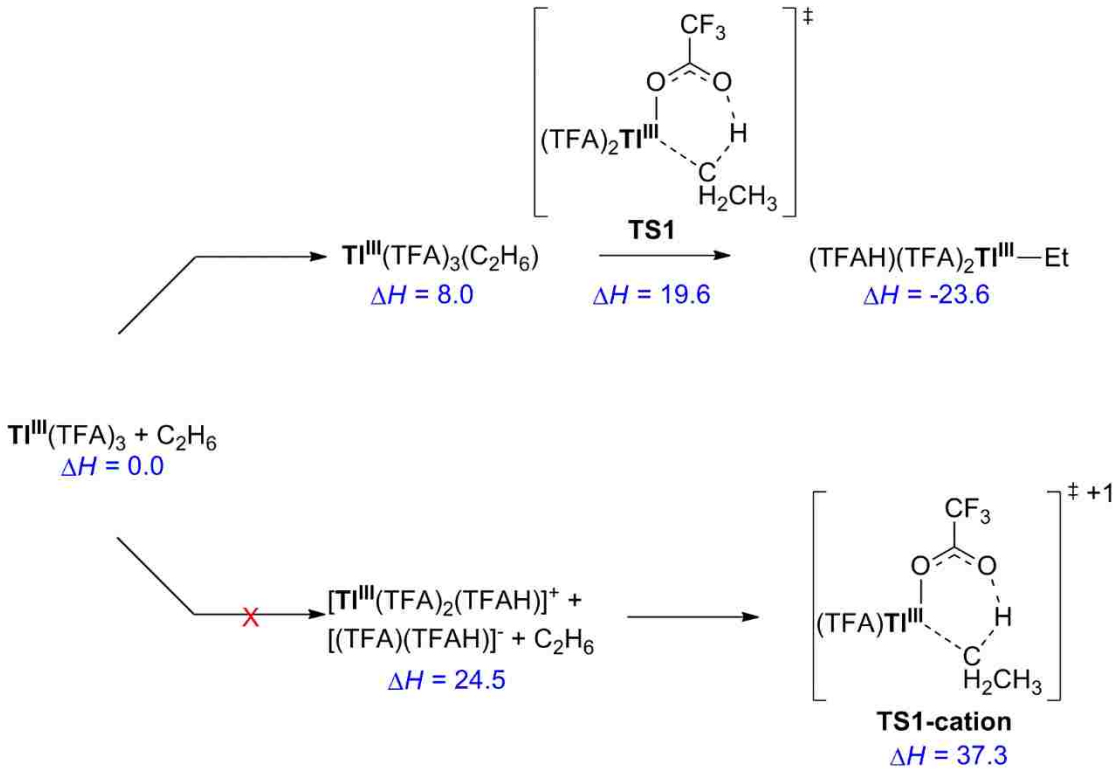

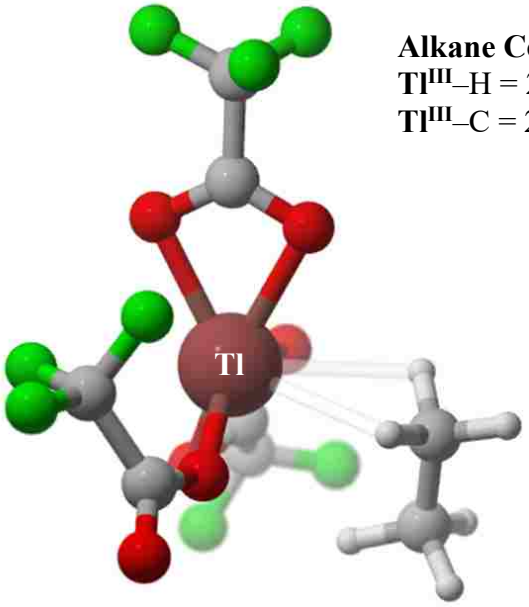

Alkane Complex
Tl^{III}–H = 2.67
Tl^{III}–C = 2.75

Figure 3-2. Model structure of the Alkane Complex. (Å)

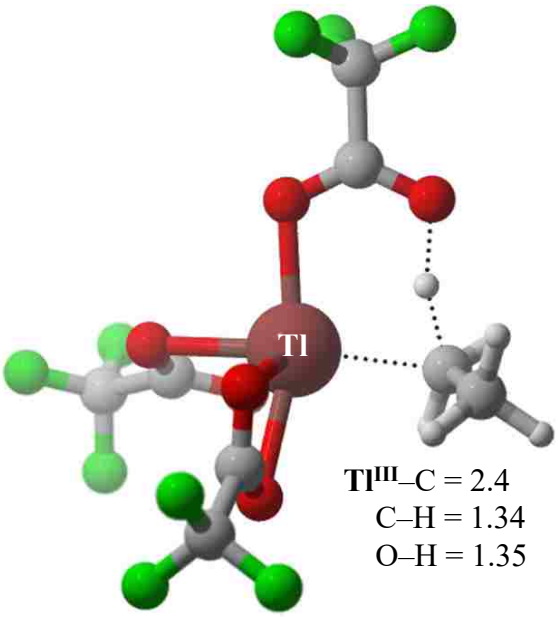

Figure 3-3. TS-1 C–H activation transition state. (Å)

A solvent proton shuttling the C–H activation transition state was also investigated (Scheme 3-9). The barrier for this transition state is similar to TS-1. This transition state is similar to TS-1 in that it forms a Tl^{III}–C while ethane is deprotonated by a TFA group; however, the TFA group does not originate from the Tl^{III} metal center. The TFA that deprotonates ethane is an explicit TFAH solvent molecule that is simultaneously deprotonated by a TFA ligand on $Tl^{III}(TFA)_3$ while it deprotonats ethane and the Tl^{III}–C bond is formed.

There is also a possibility for closed-shell C-H activation to occur from the Tl^{III} monocation ($Tl^{III}(TFA)_2^+$;Scheme 3-8) . In this case, the electrophilicity of Tl^{III} is increased, and therefore the barrier for C-H activation with $Tl^{III}(TFA)_2^+$ (TS1-cation) relative to the monocation and ethane is lower ($\Delta H^{\ddagger}$ = 12.8 kcal/mol) than TS1 (TS1 is relative to $Tl^{III}(TFA)_3$ and ethane). However, the combination of the barrier height for TS1-cation and the energy estimate for formation of the monocation results in an overall activation enthalpy of 37.3 kcal/mol (Scheme 3-8). Consequently, the lowest energy pathway for C-H oxidation involves the neutral $Tl^{III}(TFA)_3$ with ethane to form

the $(TFAH)(TFA)_2Tl(CH_2CH_3)$ intermediate through closed-shell two-electron C-H activation (TS1).

Scheme 3-9. Solvent proton shuttling C–H activation transition state.

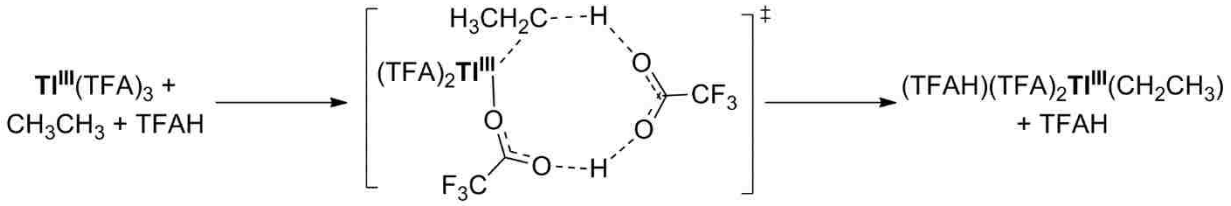

It also is possible for closed-shell C–H activation to occur from the monocation $Tl^{III}(TFA)_2^+$ (Scheme 3-8). The activation enthalpy for C–H activation with $Tl^{III}(TFA)_2^+$ (TS-1-cation) relative to the monocation and ethane is 12.8 kcal/mol. The combination of this barrier height with the energy estimate for formation of the monocation results in an overall activation enthalpy of ~37 kcal/mol. Therefore, these enthalpies suggest that the lowest energy pathway for C–H oxidation involves the neutral $Tl^{III}(TFA)_3$ with ethane to form the $(TFAH)(TFA)_2Tl^{III}$–(CH_2CH_3) intermediate through TS-1.

3.4 M–R Functionalization Mechanisms

3.4.1 Open-shell Functionalization

Scheme 3-10 outlines the homolysis of the Tl^{III}–C bond in $(TFA)_2Tl^{III}$–CH_2CH_3 to initiate a radical M–R functionalization pathway. The formation of $[Tl^{III}(TFA)_2]^\bullet$ and $[CH_2CH_3]^\bullet$ requires 50.6 kcal/mol and this is much higher in enthalpy than the closed-shell mechanisms described below.

Scheme 3-10. **Open-shell M–R functionalization pathway examined.**

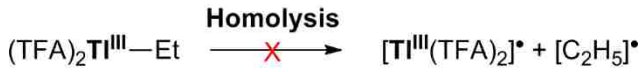

3.4.2 Closed-shell M–R Functionalization

Scheme 3-11 outlines three possible closed-shell M–R functionalization pathways. Pathway A depicts the heterolysis of the Tl^{III}–C bond to form the $[Tl^{III}(TFA)_2]^-$ anion and $[C_2H_5]^+$ cation and requires ΔH = 23.9 kcal/mol. While this result is much lower than the open-shell homolytic pathway, it is much higher in energy than pathways B and C in Scheme 3-11. This, however, does not completely rule out a heterolytic pathway because there is another pathway for Tl^{III}–C heterolysis that involves the initial loss of a TFA anion. Tl^{III} has a large reduction potential, and removing a TFA ligand to form the $[(TFA)Tl^{III}–CH_2CH_3]^+$ cation would increase the polarity of the Tl^{III}–C bond and allow the Tl^{III}–C bond to easily break heterolyticlly to form the $(TFA)Tl^{I}$ complex and ethyl cation. The ΔH for loss of a TFA anion and the formation of the $[(TFA)(TFAH)Tl^{III}–CH_2CH_3]^+$ cation and $[(TFA)(TFAH)]^-$ anion is 19.1 kcal/mol and Tl^{III}–C bond heterolysis of this complex requires less than 2 kcal/mol; but never-the-less, the energy for TFA ligand dissociation is still higher in enthalpy than the alternative functionalization pathways displayed in B and C of Scheme 3-11. Therefore, the functionalization pathway does not occur by heterolysis.

Scheme 3-11. Closed-shell M–R functionalization pathways examined

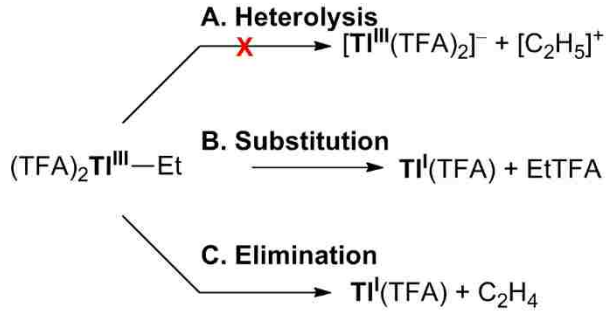

As alternatives to homolytic and heterolytic pathways, Scheme 3-11 pathways B and C summarize two competitive, lower energy closed-shell pathways for Tl^{III}–C functionalization. Scheme 3-11B outlines the lowest energy functionalization pathway for the formation of the

Tl^{I}(TFA) and EtTFA products. TS-Sub in Figure 3-4 shows the transition state for this pathway. This transition is similar to a front-side S_N2 transition state. TS-Sub utilizes the pendent oxygen atom of a TFA group to attack the Tl^{III}–C bond. Simultaneously, the (TFA)(TFAH)Tl^{III} complex is reduced to (TFA)(TFAH)Tl^{I}. The $\Delta H^{\ddagger}$ for TS-Sub is –11.7 kcal/mol relative to $Tl^{III}(TFA)_3$ and ethane and $\Delta H^{\ddagger}$ = 11.8 kcal/mol relative to the Tl^{III}–CH_2CH_3 intermediate. This low energy M–R functionalization barrier is greater than 10 kcal/mol lower in energy than heterolysis fragmentation of the Tl^{III}–C bond. This transition state is also lower in energy than the back-side S_N2 transition state where a TFA ligand completely dissociates from the Tl^{III} metal center. There is also the possibility of a three centered reductive elimination transition state similar to TS-Sub except that the TFA oxygen that is coordinated directly to Tl^{III} is involved in bond formation with the ethyl carbon atom. This transition state has a $\Delta H^{\ddagger}$ of –11.1 kcal/mol and is likely competitive with TS-Sub.

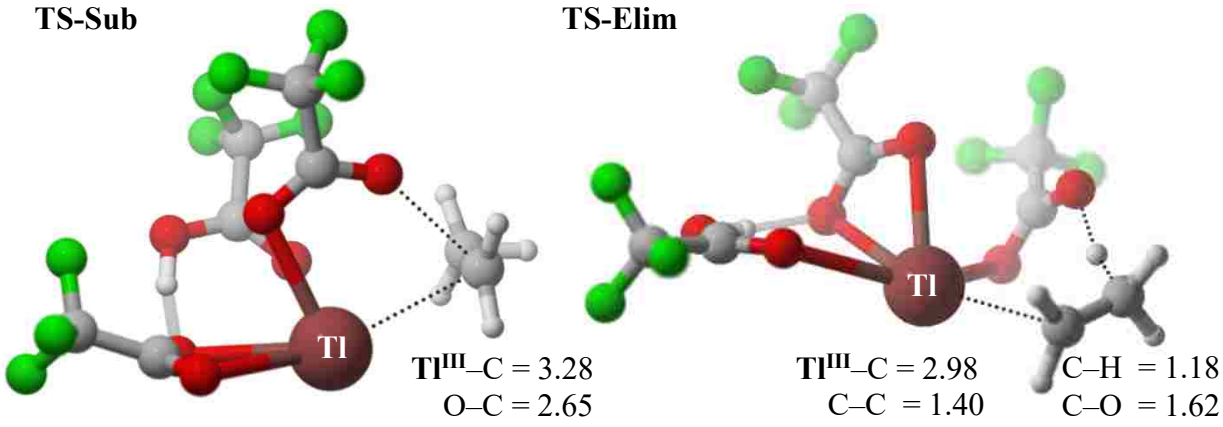

Figure 3-4. M–R functionalization transition states. (Å)

In addition to the substitution pathway, there is also a competitive elimination mechanism that forms ethylene (Scheme 3-11C). The transition state for elimination (TS-Elim, Figure 3-4) occurs by the pendant oxygen of the TFA anion deprotonating the ethyl group to form ethylene and (HTFA)(TFA)Tl^{I}. The IRC for TS-Elim confirms that ethylene dissociates from the

(TFAH)$(TFA)_2Tl^{III}$–CH_2CH_3 complex and the Tl^{III} complex is reduced to Tl^{I} if formed. The $\Delta H^{‡}$ for TS-Elim is –10.5 kcal/mol relative to reactants and 13.1 kcal/mol relative to the Tl^{III}–CH_2CH_3 intermediate.

The barrier difference between the substitution and elimination pathways is ~1 kcal/mol. Assuming that ethylene is further oxidized to $EG(TFA)_2$, the small barrier difference between TS-Sub and TS-Elim is consistent with the mixture of products (EtTFA and $EG(TFA)_2$) shown in (Scheme 3-1); the formation of EtTFA is the major product and $EG(TFA)_2$ is the minor product. There is also the possibility of EtTFA formation from solvent addition to ethylene. However, the concerted transition state for TFAH addition to ethylene has $\Delta H^{‡}$ = 23.3 kcal/mol and indicates that this process is slow in comparison to $EG(TFA)_2$ formation, as described below.

3.5 Ethylene Bistrifluoroaceticacid Formation

There are several studies that show that Tl^{III} acetates react rapidly with alkenes.[56-58] For example, Kruse and Bednarski observed a hydroxythallation product for isobutylene reaction with $Tl^{III}(OAc)_3$[59] and Grinstead saw the formation of glycols from a $Tl^{III}(OAc)_3$ and water system.[56] Just like the fast reactivity of Tl^{III} complexes and alkenes in these studies, there is a low barrier for ethylene oxidation by $Tl^{III}(TFA)_3$.

Scheme 3-12 illustrates two pathways for the formation of $EG(TFA)_2$: 1) oxidation of ethylene with a second equivalent of $Tl^{III}(TFA)_3$ and 2) C–H activation and functionalization of the EtTFA product. Ethylene oxidation by $Tl^{III}(TFA)_3$ begins with the addition of ethylene across the Tl^{III}–TFA bond to generate $(TFA)_2Tl^{III}$–CH_2CH_2TFA (ΔH = –24.4 kcal/mol). The transition state (TS-Add) shows ethylene forming a Tl^{III}–C bond and an O–C bond with the pendant oxygen of a TFA anion. The $\Delta H^{‡}$ for TS-Add is 4.3 kcal/mol relative to the $Tl^{III}(TFA)_3$(ethylene) complex.

Scheme 3-12. Outline of ethylene oxidation mechanism. (kcal/mol)

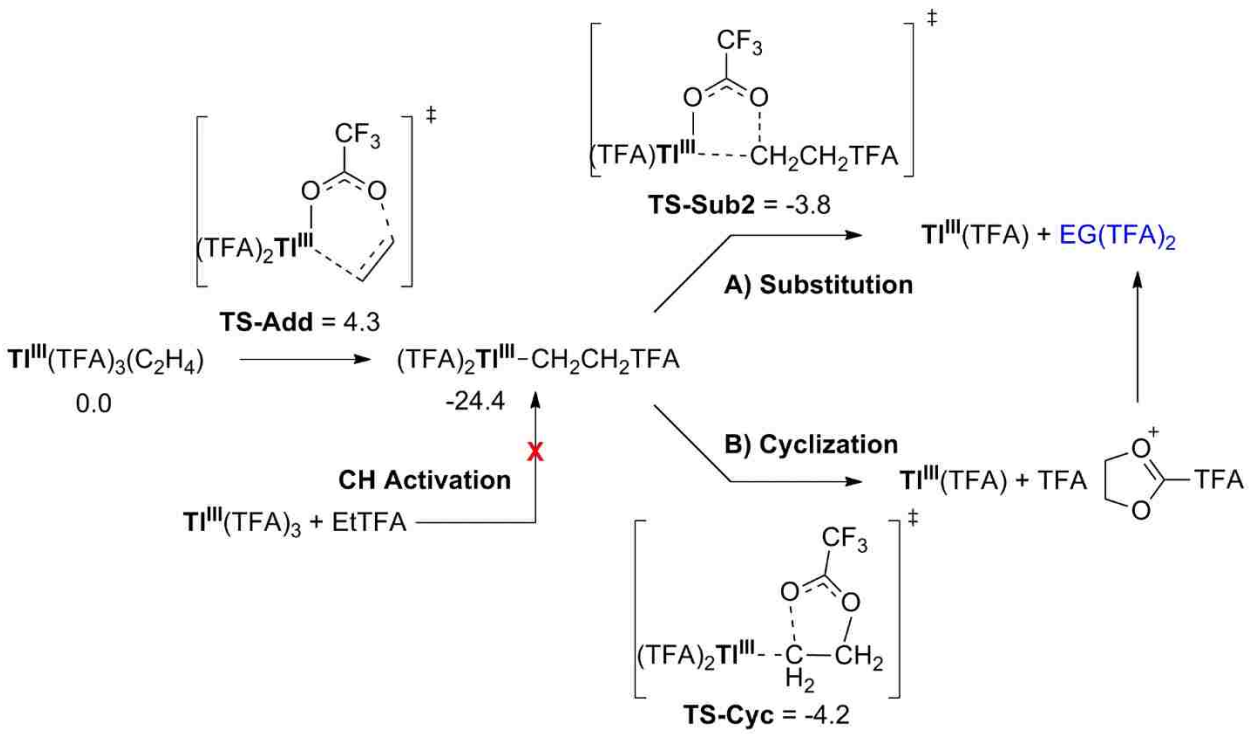

Functionalization of the $(TFA)_2Tl^{III}$–CH_2CH_2TFA intermediate occurs by two competitive pathways. Scheme 3-12A involves a substitution transition state (TS-Sub2) similar to M–R functionalization of the Tl^{III}–CH_2CH_3 intermediate and the $\Delta H^{\ddagger}$ for this transition state is 20.6 kcal/mol relative to $(TFA)_2Tl^{III}$–CH_2CH_2TFA. There is also the possibility that a TFA ligand can act as an internal nucleophile and react with itself to form a cyclic $CH_2CH_2TFA^+$ cation. This transition state has a $\Delta H^{\ddagger}$ value less than 1 kcal/mol lower in energy than TS-Sub2, showing that these two methods are competitive and, therefore, both are likely pathways. The formation of a cyclic $CH_2CH_2TFA^+$ cation leads to ejection of $Tl^{I}(TFA)$ and TFA. $EG(TFA)_2$ is then generated by the TFA anion attacking the cyclic $CH_2CH_2TFA^+$ cation.

The second pathway for $EG(TFA)_2$ product formation is by oxidation of the EtTFA product to form the $(TFA)_2Tl^{III}$–CH_2CH_2TFA intermediate. The $\Delta H^{\ddagger}$ for C–H activation of EtTFA by $Tl^{III}(TFA)_3$ is 24.6 kcal/mol. This barrier is ~5 kcal/mol higher than C–H activation of ethane and

therefore $EG(TFA)_2$ is not generated from oxidation of the EtTFA product and EtTFA is protected from overoxidation.

3.6 Conclusion

DFT calculations indicate that alkane oxidation by $Tl^{III}(TFA)_3$ involves electrophilic C–H activation followed by M–R functionalization. M–R functionalization involves two competitive substitution and elimination pathways that result in EtTFA product and $EG(TFA)_2$. EtTFA does not undergo further oxidation by $Tl^{III}(TFA)_3$ because C–H activation to form $(TFA)_2Tl^{III}$–CH_2CH_2TFA is significantly higher in energy than C–H activation of ethane.

3.7 References

(1) Konnick, M. M.; Bischof, S. M.; Yousufuddin, M.; Hashiguchi, B. G.; Ess, D. H.; Periana, R. A. *J. Am. Chem. Soc* **2014**, *136*, 10085.

(2) Periana, R. A.; Taube, D. J.; Gamble, S.; Taube, H.; Satoh, T.; Fujii, H. *Science* **1998**, *280*, 560.

(3) Zerella, M.; Bell, A. T. *J. Mol. Catal. A-Chem.* **2006**, *259*, 296.

(4) Ahrens, S.; Strassner, T. *Inorg. Chim. Acta* **2006**, *359*, 4789.

(5) Periana, R. A.; Mironov, O.; Taube, D.; Bhalla, G.; Jones, C. *Science* **2003**, *301*, 814.

(6) Zerella, M.; Mukhopadhyay, S.; Bell, A. T. *Chem. Commun.* **2004**, 1948.

(7) Ahrens, S.; Zeller, A.; Taige, M.; Strassner, T. *Organometallics* **2006**, *25*, 5409.

(8) Zerella, M.; Kahros, A.; Bell, A. T. *J. Catal.* **2006**, *237*, 111.

(9) Remy, M. S.; Cundari, T. R.; Sanford, M. S. *Organometallics* **2010**, *29*, 1522.

(10) McCall, A. S.; Wang, H.; Desper, J. M.; Kraft, S. *J. Am. Chem. Soc* **2011**, *133*, 1832.

(11) Munz, D.; Meyer, D.; Strassner, T. *Organometallics* **2013**, *32*, 3469.

(12) Munz, D.; Strassner, T. *Top. Catal.* **2014**, *57*, 1372.

(13) Munz, D.; Strassner, T. *Chem. -Eur. J.* **2014**, *20*, 14872.

(14) Chen, H.; Schlecht, S.; Semple, T. C.; Hartwig, J. F. *Science* **2000**, *287*, 1995.

(15) Hartwig, J. F.; Cook, K. S.; Hapke, M.; Incarvito, C. D.; Fan, Y.; Webster, C. E.; Hall, M. B. *J. Am. Chem. Soc* **2005**, *127*, 2538.

(16) O'Reilly, M. E.; Pahls, D. R.; Cundari, T. R.; Gunnoe, T. B. *Organometallics* **2014**, *33*, 6504.

(17) Fu, R.; Nielsen, R. J.; Goddard, W. A.; Fortman, G. C.; Gunnoe, T. B. *ACS Catal.* **2014**, *4*, 4455.

(18) Vetter, A. J.; Flaschenriem, C.; Jones, W. D. *J. Am. Chem. Soc* **2005**, *127*, 12315.

(19) George, M. W.; Hall, M. B.; Jina, O. S.; Portius, P.; Sun, X.-Z.; Towrie, M.; Wu, H.; Yang, X.; Zarić, S. D. *Proc. Natl. Acad. Sci. USA.* **2010**, *107*, 20178.

(20) George, M. W.; Hall, M. B.; Portius, P.; Renz, A. L.; Sun, X.-Z.; Towrie, M.; Yang, X. *Dalton Trans.* **2011**, *40*, 1751.

(21) Niu, S.; Hall, M. B. *J. Am. Chem. Soc* **1999**, *121*, 3992.

(22) Janowicz, A. H.; Bergman, R. G. *J. Am. Chem. Soc* **1982**, *104*, 352.

(23) Janowicz, A. H.; Bergman, R. G. *J. Am. Chem. Soc* **1983**, *105*, 3929.

(24) Young, K. J. H.; Oxgaard, J.; Ess, D. H.; Meier, S. K.; Stewart, T.; Goddard III, W. A.; Periana, R. A. *Chem. Commun.* **2009**, 3270.

(25) Goldman, A. S.; Roy, A. H.; Huang, Z.; Ahuja, R.; Schinski, W.; Brookhart, M. *Science* **2006**, *312*, 257.

(26) Choi, J.; MacArthur, A. H. R.; Brookhart, M.; Goldman, A. S. *Chem. Rev.* **2011**, *111*, 1761.

(27) Choi, J.; Wang, D. Y.; Kundu, S.; Choliy, Y.; Emge, T. J.; Krogh-Jespersen, K.; Goldman, A. S. *Science* **2011**, *332*, 1545.

(28) Haibach, M. C.; Kundu, S.; Brookhart, M.; Goldman, A. S. *Acc. Chem. Res.* **2012**, *45*, 947.

(29) Findlater, M.; Choi, J.; Goldman, A.; Brookhart, M. In *Alkane C-H Activation by Single-Site Metal Catalysis*; Pérez, P. J., Ed.; Springer Netherlands: 2012; Vol. 38, p 113.

(30) Abu-Hasanayn, F.; Krogh-Jespersen, K.; Goldman, A. S. *J. Am. Chem. Soc* **1993**, *115*, 8019.

(31) Abu-Hasanayn, F.; Krogh-Jespersen, K.; Goldman, A. S. *Inorg. Chem.* **1993**, *32*, 495.

(32) Biswas, S.; Huang, Z.; Choliy, Y.; Wang, D. Y.; Brookhart, M.; Krogh-Jespersen, K.; Goldman, A. S. *J. Am. Chem. Soc* **2012**, *134*, 13276.

(33) Cheng, C.; Kim, B. G.; Guironnet, D.; Brookhart, M.; Guan, C.; Wang, D. Y.; Krogh-Jespersen, K.; Goldman, A. S. *J. Am. Chem. Soc* **2014**, *136*, 6672.

(34) Krogh-Jespersen, K.; Czerw, M.; Summa, N.; Renkema, K. B.; Achord, P. D.; Goldman, A. S. *J. Am. Chem. Soc* **2002**, *124*, 11404.

(35) Krogh-Jespersen, K.; Czerw, M.; Goldman, A. S. *J. Mol. Catal. A-Chem.* **2002**, *189*, 95.

(36) Krogh-Jespersen, K.; Czerw, M.; Zhu, K.; Singh, B.; Kanzelberger, M.; Darji, N.; Achord, P. D.; Renkema, K. B.; Goldman, A. S. *J. Am. Chem. Soc* **2002**, *124*, 10797.

(37) Kundu, S.; Choi, J.; Wang, D. Y.; Choliy, Y.; Emge, T. J.; Krogh-Jespersen, K.; Goldman, A. S. *J. Am. Chem. Soc* **2013**, *135*, 5127.

(38) Kundu, S.; Choliy, Y.; Zhuo, G.; Ahuja, R.; Emge, T. J.; Warmuth, R.; Brookhart, M.; Krogh-Jespersen, K.; Goldman, A. S. *Organometallics* **2009**, *28*, 5432.

(39) Zhu, K.; Achord, P. D.; Zhang, X.; Krogh-Jespersen, K.; Goldman, A. S. *J. Am. Chem. Soc* **2004**, *126*, 13044.

(40) Hartwig, J. F. *Acc. Chem. Res.* **2012**, *45*, 864.

(41) Hashiguchi, B. G.; Konnick, M. M.; Bischof, S. M.; Gustafson, S. J.; Devarajan, D.; Gunsalus, N.; Ess, D. H.; Periana, R. A. *Science* **2014**, *343*, 1232.

(42) Elson, I. H.; Kochi, J. K. *J. Am. Chem. Soc* **1973**, *95*, 5060.

(43) Lau, W.; Kochi, J. K. *J. Am. Chem. Soc* **1984**, *106*, 7100.

(44) Lau, W.; Kochi, J. K. *J. Am. Chem. Soc* **1986**, *108*, 6720.

(45) McKillop, A.; Fowler, J. S.; Zelesko, M. J.; Hunt, J. D.; Taylor, E. C.; McGillivray, G. *Tetrahedron Lett.* **1969**, *10*, 2423.

(46) McKillop, A.; Hunt, J. D.; Zelesko, M. J.; Fowler, J. S.; Taylor, E. C.; McGillivray, G.; Kienzle, F. *J. Am. Chem. Soc* **1971**, *93*, 4841.

(47) Taylor, E. C.; McKillop, A.; Hunt, J. D.; Naylor, R. D. *J. Am. Chem. Soc* **1971**, *93*, 4918.

(48) Periana, R. A.; Taube, D. J.; Evitt, E. R.; Löffler, D. G.; Wentrcek, P. R.; Voss, G.; Masuda, T. *Science* **1993**, *259*, 340.

(49) Faggiani, R.; Brown, I. D. *Acta Crystallogr., Sect. B* **1978**, *B34*, 2845.

(50) Briody, J.; Moore, R. *Chem. Ind.* **1970**, 803.

(51) Lau, W.; Huffman, J. C.; Kochi, J. K. *J. Am. Chem. Soc* **1982**, *104*, 5515.

(52) Kwok, P. Y.; Stock, L. M.; Wright, T. L. *J. Org. Chem.* **1979**, *44*, 2309.

(53) Henry, P. M. *J. Org. Chem.* **1970**, *35*, 3083.

(54) Briody, J. M.; Moore, R. A. *J. Chem. Soc. Perk. Trans. 2* **1972**, 179.

(55) McKillop, A.; Taylor, E. C. *Adv. Organomet. Chem.* **1973**, 147.

(56) Grinstead, R. *J. Org. Chem.* **1961**, *26*, 238.

(57) Henry, P. M. *J. Am. Chem. Soc* **1965**, *87*, 4423.

(58) Pande, K. C.; Winstein, S. *Tetrahedron Lett.* **1964**, *5*, 3393.

(59) Kruse, W.; Bednarski, T. M. *J. Org. Chem.* **1971**, *36*, 1154.

4 COMPARISON OF TL^{III} TO HG^{II} AND IR^{III} FOR REACTIVITY AND PARTIAL OXIDATION SELECTIVITY FOR ALKANE C–H FUNCTIONALIZATION

4.1 Introduction

Recently, the Periana and Ess groups disclosed the partial oxidation of light alkanes by the p-block main-group metal complex thallium(III) tristrifluoroacetate ($Tl^{III}(TFA)_3$; Equation 4-1). A two-electron closed-shell C–H activation and functionalization mechanism was proposed based on DFT calculations and experiment (Chapter 3).[1] The discovery that 6th-row main-group trifluoroacetates efficiently promote alkane trifluoroacetoxylation in trifluoroacetic acid (TFAH) solvent by two-electron C–H activation/functionalization mechanism is significant for several reasons: 1) alkanes are oxidized in carboxylic acid solvent rather than superacid solvent;[1-15] 2) $Co^{III}(TFA)_3$, a transition-metal complex with the same oxidation state and TFA ligands, oxidizes alkanes via a radical mechanism;[16-19] 3) $Hg^{II}(TFA)_2$ does not functionalize light alkanes.[1,7] 4) $Tl^{III}(TFA)_3$ oxidizes arenes via a radical mechanism;[20-23] and 5) the alkyl trifluoroacetate ester products are stable towards overoxidation.

$$Tl^{III}(TFA)_3 + C_2H_6 \xrightarrow[TFAH]{} MeTFA + TFAH + Tl^{I}(TFA) \qquad 4\text{-}1$$

In this chapter, density functional theory (DFT) calculations are presented to develop a reactivity model and origin of partial oxidation selectivity for alkanes by $Tl^{III}(TFA)_3$. This chapter also compares the reactivity and energy landscape of $Tl^{III}(TFA)_3$ to a transition metal, $Ir^{III}(TFA)_3$, with the same oxidation state and ligands. Lastly, this chapter provides details of why $Hg^{II}(TFA)_2$ is less reactive than $Tl^{III}(TFA)_3$.

4.2 Qualitative Reactivity of Tl^{III}

The qualitative energy landscape, based on DFT calculations presented in Chapter 3, for C–H activation and metal–alkyl (M–R) functionalization of ethane by $Tl^{III}(TFA)_3$ is displayed in Scheme 4-1. The shape of this landscape is consistent with and explains the experimental observation that there is no C–H to C–D exchange when reactions are found in deuterated trifluoroacetic acid (TFAD). The lack of H/D exchange results from a much smaller barrier for M–R functionalization from the $(TFAH)(TFA)_2Tl^{III}–CH_2CH_3$ intermediate compared to the larger barrier for protonation/deuteration of the $(TFAH)(TFA)_2Tl^{III}–CH_2CH_3$ intermediate. Formation of EtTFA and $Tl^{I}(TFA)$ from M–R functionalization is highly exothermic and irreversible.

The electronic configuration for Tl^{III} in $Tl^{III}(TFA)_3$ is $[Xe]4f^{14}5d^{10}$. Figure 4-1 displays the M06 highest occupied molecular orbital (HOMO) and lowest occupied molecular orbital (LUMO). The low-energy HOMO and LUMO orbitals and large reduction potential indicates that Tl^{III} is highly electrophilic. The LUMO orbital is mainly composed of a 6s orbital with antibonding interactions with the TFA ligands. The HOMO, which is close in energy to other occupied orbitals, is mainly composed of nonbonding TFA ligand orbitals. The d^{10} electrons in the HOMO are ~6 eV lower in energy than the LUMO, indicating these orbitals are core-like orbitals rather than valence orbitals.

Scheme 4-1. Qualitative C–H activation and functionalization energy landscape for oxidation of ethane by $Tl^{III}(TFA)_3$.

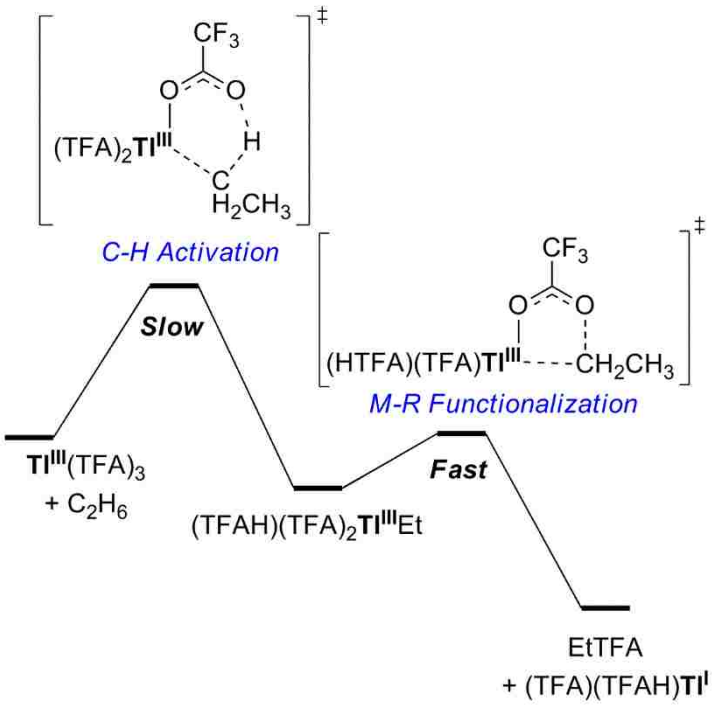

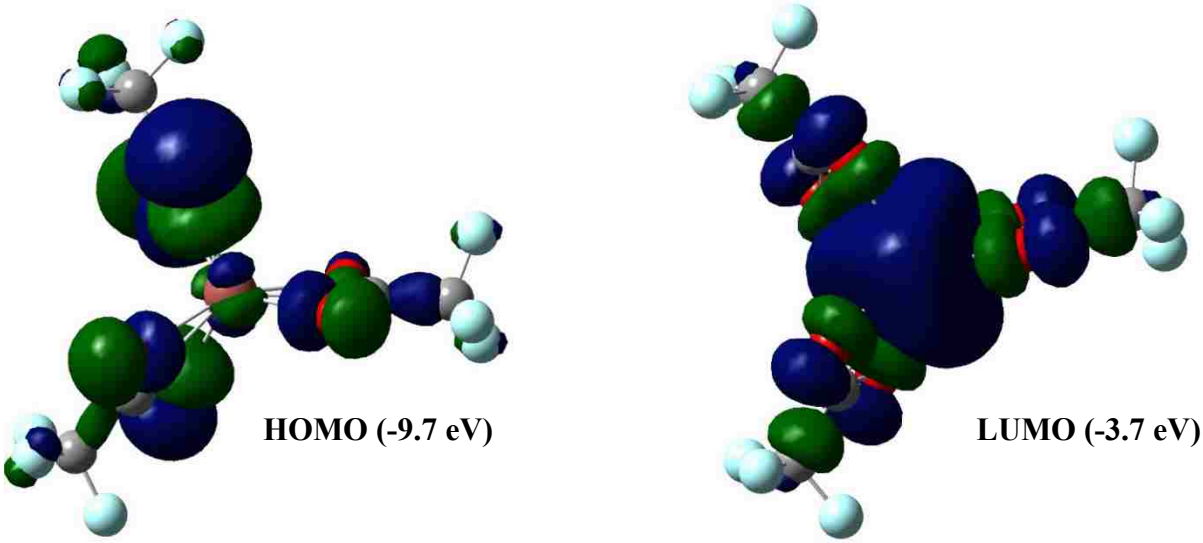

Figure 4-1. HOMO and LUMO orbitals for $Tl^{III}(TFA)_3$.

Figure 1-2 presents a qualitative frontier orbital interaction analysis for the C–H activation transition state of ethane by $Tl^{III}(TFA)_3$. Forward-bonding occurs from the overlap of the filled C–

H bond of ethane with the vacant 6s orbital of Tl^{III} and results in the Tl^{III}–C bond. Gross orbital population analysis of the fragments of the C–H activation transition state indicates that Tl^{III} has very little sp hybridization and this frontier perspective likely portrays the transition state interaction. This forward-bonding interaction dominates over back-bonding due to the low energy LUMO. The back-bonding orbital interaction occurs between the nonbonding electron pair of a TFA ligand and the empty C–H σ* orbital. Again, this indicates that formation of the Tl^{III}–C bond is significantly more important than proton transfer (Scheme 1-2); the Tl^{III} metal acidifies the alkane C–H bond; therefore, this reaction should be called an electrophilic C–H activation. The dominant forward-bonding orbital interaction was confirmed by energy decomposition analysis (EDA) calculations performed on the C–H activation transition state. EDA also revealed that stabilizing bonding interactions in the transition state are composed of covalent (orbital) and electrostatic interactions.[24]

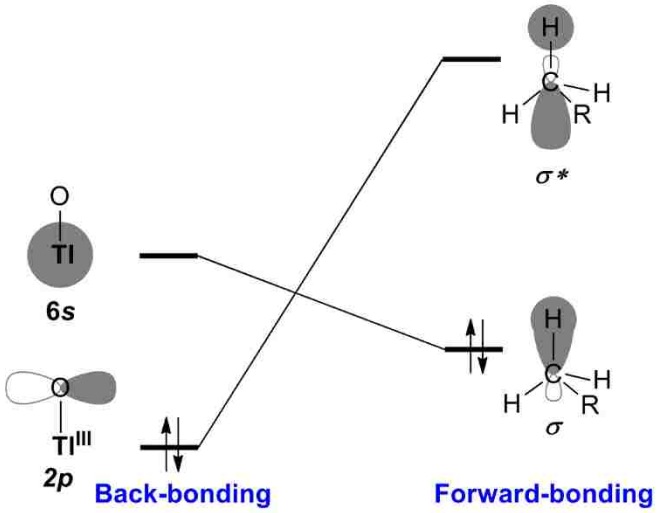

Figure 4-2. Tl^{III} frontier orbital interactions involved in C–H activation.

Scheme 4-2. Qualitative transition-state reactivity model.

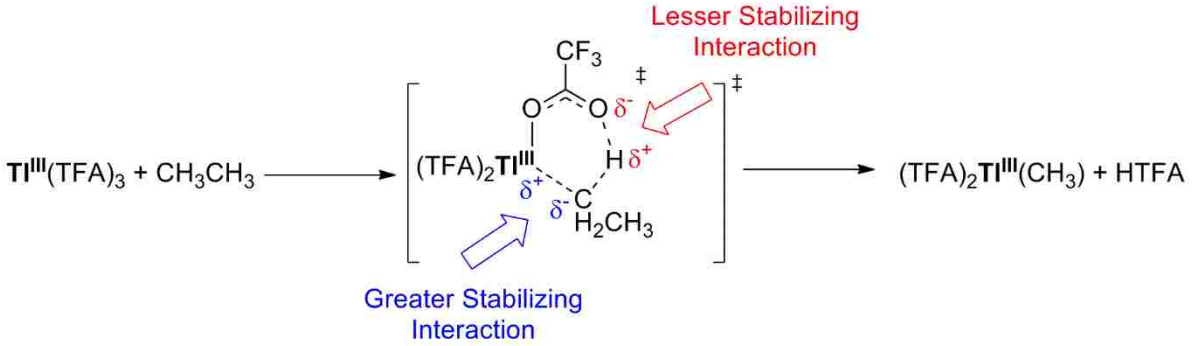

The transition-state reactivity model in Scheme 4-2 also provides an explanation for the lesser C–H activation reactivity of EtTFA with $Tl^{III}(TFA)_3$ and prevention of overoxidation. As described in Chapter 3, EtTFA is protected from overoxidation due to a ~5 kcal/mol larger enthalpy barrier for C–H activation compared to ethane. While the idea of electron-withdrawing groups raising the activation barrier for electrophilic C–H activation is not new, the quantitative magnitude of the TFA group was not anticipated. It is generally assumed that only very strong electron-withdrawing groups, such as bisulfate, prevent alkane overoxidation.[6,25-28] This could be considered paradoxical since the pK_a for EtTFA is lower than ethane. However, the much more dominant forward-bonding orbital interaction shown in Scheme 4-2 is responsible for relative reactivity. For EtTFA, the C–H bond HOMO is lower in energy compared to the C–H bond HOMO of ethane, and therefore there is a larger frontier orbital energy gap for EtTFA.

Stronger C–H bonds generally correlate with stronger M–R bonds after C–H activation.[16,34,35] The calculated bond dissociation enthalpies for ethane and EtTFA are 100.8 and 101.8 kcal/mol respectively. The Tl^{III}–CH_2CH_3 bond dissociation enthalpy is 50.6 kcal/mol and the Tl^{III}–CH_2CH_2TFA bond dissociation enthalpy is 51.7 kcal/mol. Therefore, M–R bond strengths do not play a significant role in the transition state for determining the relative barrier heights of ethane and EtTFA.

4.3 Comparison of Tl^{III} versus Ir^{III} C–H Activation

$Ir^{III}(TFA)_3$ was chosen as a transition metal comparison to $Tl^{III}(TFA)_3$ for several reasons: 1) $Ir^{III}(OAc)_3$ is known to activate and functionalize C–H bonds of alkanes;[29,30] 2) both Ir^{III} and Tl^{III} metal centers have formal +3 oxidation states; 3) it is possible to computationally locate ground-state and transition-state structures for $Ir^{III}(TFA)_3$ that are very similar to the structures for $Tl^{III}(TFA)_3$ (Figure 4-3).

The slight differences in the Tl^{III} and Ir^{III} structures are due to the difference in d-electron count ($Ir^{III} = d^6$, $Tl^{III} = d^{10}$) and the LUMO orbital. As described in Section 4.2, the LUMO for Tl^{III} that interacts with the TFA and carbon ligands is the more polarized 6s orbital. In contrast, Ir^{III} utilizes a more directional unoccupied 5d orbital. The Ir^{III} structures appear to exhibit a strong trans effect (Figure 4-3).

Despite somewhat similar transition-state and ground-state geometries, the energetics for ethane C–H activation and M–R functionalization are markedly different for $Ir^{III}(TFA)_3$ compared to $Tl^{III}(TFA)_3$. Scheme 4-3 displays these differences by comparing the enthalpy landscapes for C–H activation and M–R functionalization of $Ir^{III}(TFA)_3$ and $Tl^{III}(TFA)_3$ reactions with ethane. $Ir^{III}(TFA)_3$ has a lower barrier for C–H bond activation than $Tl^{III}(TFA)_3$, which could be due to the more directional Ir^{III} 5d orbital and less directional Tl^{III} 6s orbital.

The M–R functionalization barriers show the opposite order of barrier heights. The M–R functionalization transition state that leads to EtTFA from $(TFAH)(TFA)_2Ir^{III}–CH_2CH_3$ requires an activation enthalpy of greater than 60 kcal/mol. The Tl^{III} functionalization transition state requires an activation enthalpy of only 12 kcal/mol. The low-energy M–R functionalization pathway of the Tl^{III}–C intermediate is likely due to the highly polarized $M^{\delta-}–R^{\delta+}$ bond and the much larger two-electron reduction potential. This bond polarization is opposite to low oxidation state transition-metal carbon bond polarization, $M^{\delta+}–R^{\delta-}$. This comparison of the $Tl^{III}(TFA)_3$ and

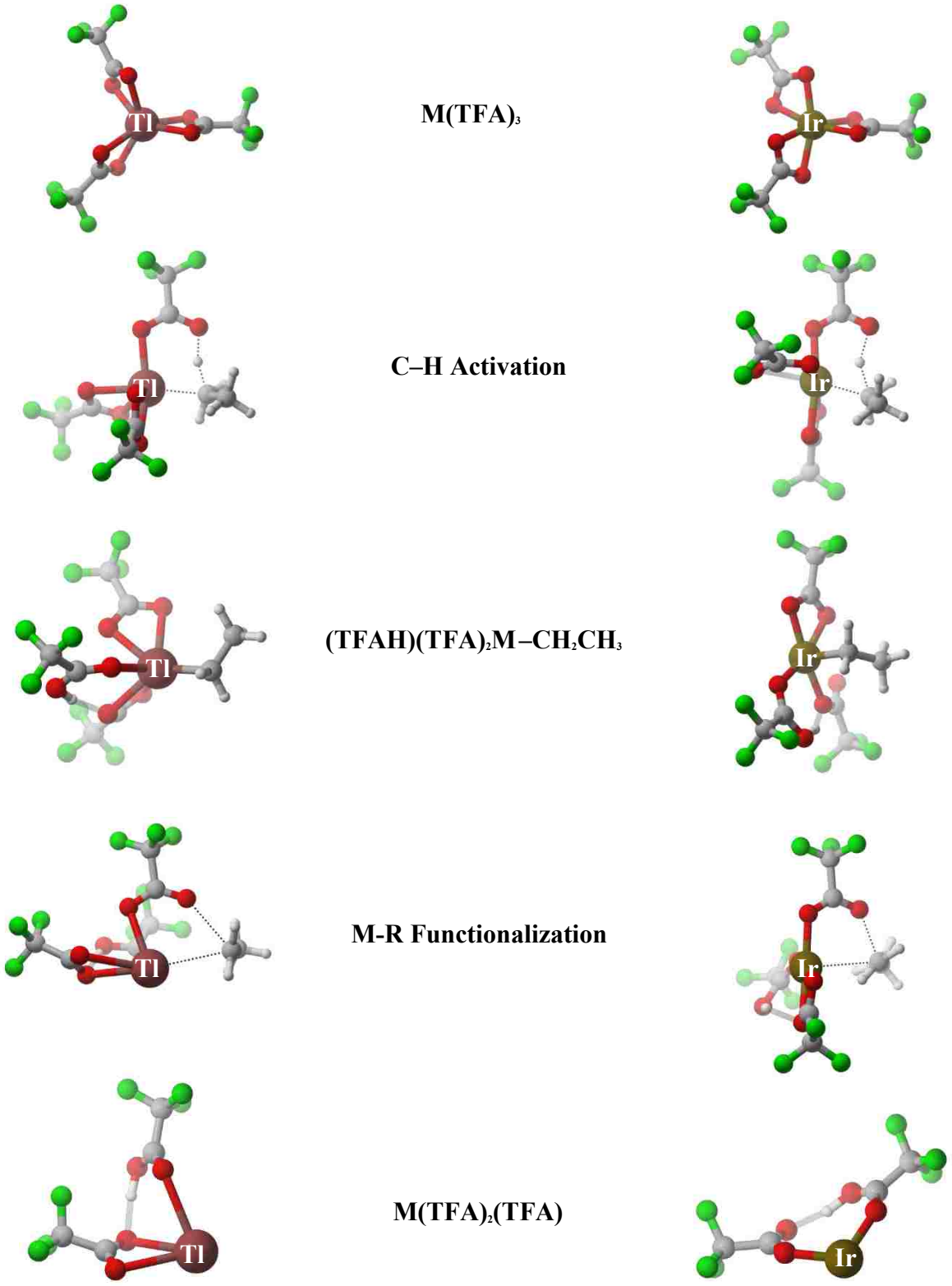

Figure 4-3. Geometries for the C–H activation and functionalization geometries of Ir^{III} and Tl^{III}. (M = Tl^{III} or Ir^{III})

$Ir^{III}(TFA)_3$ pathways suggests that the success of Tl^{III} and other highly electrophilic main-group metals for C–H bond oxidation of alkanes is the ability to have a moderately low energy C–H activation transition state with highly electrophilic metal centers due to the lack of ligand field stabilization energy and a highly polarized $M^{\delta-}$–$C^{\delta+}$ intermediate to facilitate the rapid M–R functionalization pathway.

Scheme 4-3. Comparison of energy landscapes for Tl^{III} and Ir^{III} C–H activation and functionalization with ethane.

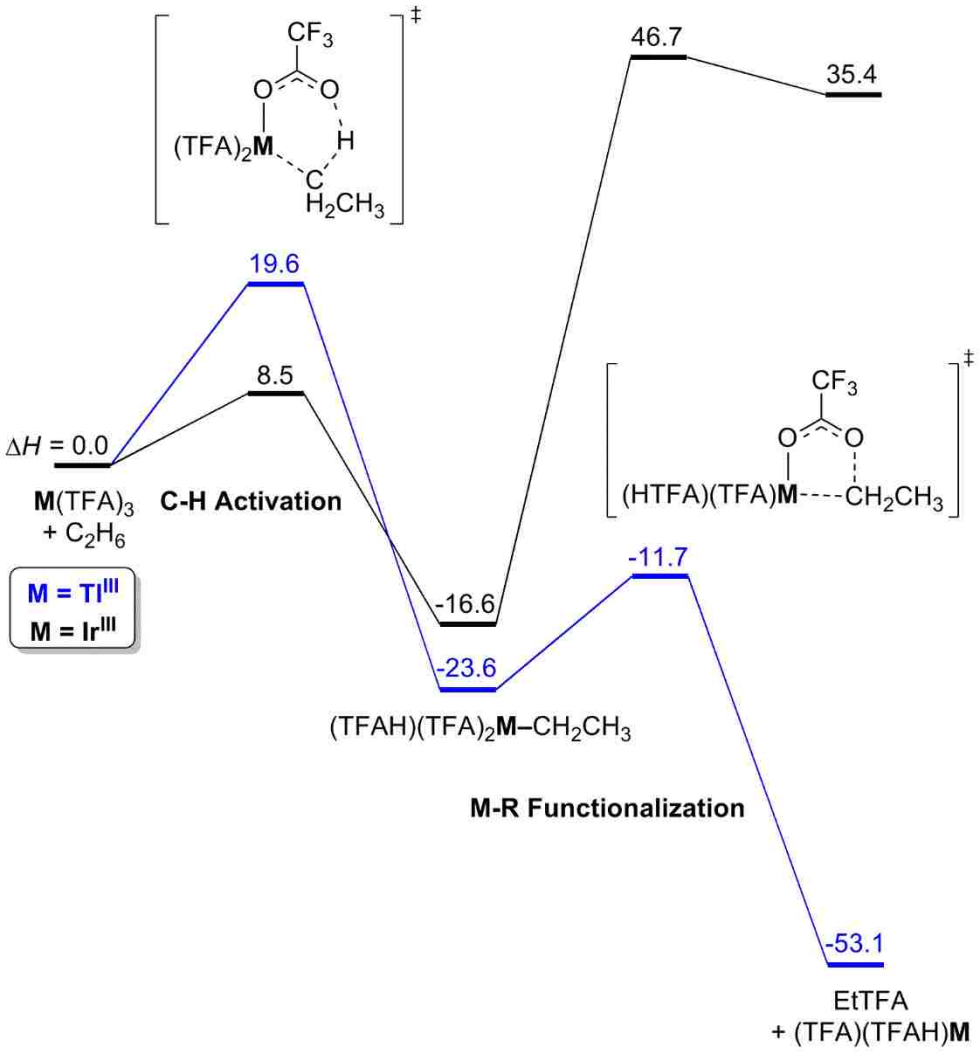

4.4 Comparison of Tl^{III} to Hg^{II}

As discussed in Section 4.1, $Tl^{III}(TFA)_3$ oxidation of methane and ethane was somewhat unexpected because $Hg^{II}(TFA)_2$ is unreactive towards alkanes.[1,7] To compare $Tl^{III}(TFA)_3$ versus $Hg^{II}(TFA)_2$, the activation barriers for methane C–H activation were calculated. The $Hg^{II}(TFA)_2$ ground state is displayed in Figure 4-4, and the C–H activation transition state is displayed in Figure 4-5. The transition state located for $Hg^{II}(TFA)_2$ is similar to previous structures reported by Cundari[31] and speculated by Winstein and others.[32,33]

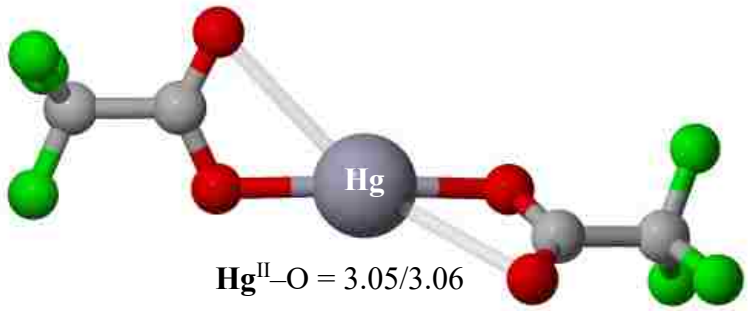

Figure 4-4. Hg^{II} ground state and methane C–H activation transition state. (Å)

These structures are consistent with the expected lack of reactivity for Hg^{II}. The barrier for $Hg^{II}(TFA)_2$ C–H activation of methane is $\Delta H^{\ddagger}$ = 26.5 kcal/mol and $\Delta G^{\ddagger}$ = 38.9 kcal/mol. The barrier for $Tl^{III}(TFA)_3$ C–H activation of methane is $\Delta H^{\ddagger}$ = 17.7 kcal/mol; $\Delta G^{\ddagger}$ = 30.9 kcal/mol. The relatively large $\Delta G^{\ddagger}$ for C–H activation of $Hg^{II}(TFA)_2$ with methane is consistent with a complete lack of reactivity.

There are also differences in the energetics of the M–R intermediates. The ΔH for the formation of the $(TFA)Hg^{II}–CH_3$ intermediate is endothermic by 4.5 kcal/mol. The ΔH for the formation of the $(TFA)_2Tl^{III}–CH_3$ intermediate is –12.7 kcal/mol. These thermodynamic quantities could suggest that the difference in reactivity is the result of forming a stronger $Tl^{III}–CH_3$ bond versus a weaker $Hg^{II}–CH_3$ bond. However, the calculated bond dissociation enthalpies (Table 4-1)

reveal that the Hg^{II}–CH_3 bond enthalpy (ΔH = 60.7 kcal/mol) is larger than the Tl^{III}–CH_3 bond enthalpy (ΔH = 54.2 kcal/mol). This demonstrates that M–CH_3 bond strengths do not determine the relative kinetics of C–H activation.

Table 4-1. M–CH_3 and M–TFA bond dissociation enthalpies for $Tl^{III}(TFA)_3$, $Hg^{II}(TFA)_2$ (TFA)Hg^{II}–CH_3 and $(TFA)_2Tl^{III}$–CH_3 in TFAH solvent.

M−CH_3	ΔH (M• + •CH_3)	ΔH (M^+ + $^-CH_3$)	ΔH (M^- + $^+CH_3$)
(TFA)**Hg^{II}**–CH_3	60.7	116.3	98.3
$(TFA)_2$**Tl^{III}**–CH_3	54.2	140.9	55.9

M–TFA	ΔH (M• + •$OOCCF_3$)	ΔH (M^+ + $^-OOCCF_3$)
Hg^{II} $(TFA)_2$	79.8	43.8
Tl^{III} $(TFA)_3$	56.2	51.3

Table 4-1. also reports the M–TFA homolysis energies for $Hg^{II}(TFA)_2$ and $Tl^{III}(TFA)_3$. The Hg^{II}–TFA bond dissociation enthalpy is 79.8 kcal/mol and the Tl^{III}–TFA bond dissociation enthalpy is 56.2 kcal/mol. This 23.6 kcal/mol difference in bond dissociation enthalpies controls the overall thermodynamics for forming M–R intermediates.

Table 4-2. ΔG_{Solv} values for $Hg^{II}(TFA)_2$ and the C–H activation transition state for $Hg^{II}(TFA)_2$ with methane. (kcal/mol)

	ΔG_{Solv}
Hg^{II} $(TFA)_2$	–30.6
Hg^{II} $(TFA)_2$ with methane C–H Activation Transition State	–29.6

Unlike the difference in M–TFA bond dissociation enthalpies between Hg^{II} and Tl^{III}, heterolysis of the M–TFA bond is lower in energy for Hg^{II} than for Tl^{III}. Heterolysis without explicit solvation of $Hg^{II}(TFA)_2$ to form the $[Hg^{II}(TFA)]^+$ cation and TFA anion requires ΔH = 43.8 kcal/mol, while heterolysis without explicit solvation of $Tl^{III}(TFA)_3$ to form the $[Tl^{III}(TFA)_2]^+$

cation and TFA anion requires ΔH= 51.3 kcal/mol. These heterolysis energies suggest the reactivity difference between Tl^{III} and Hg^{II} because Tl^{III} is more electrophilic than Hg^{II}.

The C–H activation transition states for Tl^{III} and Hg^{II} were also computed in the gas phase (Figure 4-5) to determine the contribution of solvation to relative Tl^{III} and Hg^{II} reactivity. The C–H activation transition states for $Tl^{III}(TFA)_3$ and methane in the gas phase and TFAH solvent displayed only minor differences in the bond lengths; however, the C–H activation transition state geometries for $Hg^{II}(TFA)_2$ with methane display significant changes between the transition-state geometries in gas phase and TFAH solvent. The first noticeable change is on the spectator TFA ligand. The spectator ligand on the Hg^{II} transition state changed from a κ^1 interaction in TFAH solvent to a κ^2 interaction in the gas phase. Other changes can be seen in the TFA ligand that deprotonates methane. In TFAH solvent this TFA ligand fully dissociates, but in the gas phase the ligand remains tightly bound to the Hg^{II} metal center. These structural changes on the $Hg^{II}(TFA)_2$ and ethane C–H activation transition state lead to a slight increase for the C–H activation barrier in TFAH solvent ($\Delta H^{\ddagger}$ = 26.5 kcal/mol) compared to the C–H activation barrier in the gas phase ($\Delta H^{\ddagger}$ = 25.2 kcal/mol). This effect of solvent on the C–H activation transition state is further elucidated by the calculated ΔG_{Solv} values shown in Table 4-2. The ΔG_{Solv} of ~ –30 kcal/mol for the ground state and transition state geometries show that Hg^{II} complexes are well stabilized by TFAH solvent.

In contrast to the increase of the C–H activation barrier for $Hg^{II}(TFA)_2$ with methane in TFAH solvent, the TFAH solvent helps to decrease the C–H activation barrier for $Tl^{III}(TFA)_3$ with methane; in the gas phase, the C–H activation transition state for a $Tl^{III}(TFA)_3$ reaction with methane is $\Delta H^{\ddagger}$ = 22.5 kcal/mol and this decreases to $\Delta H^{\ddagger}$ = 17.7 kcal/mol in TFAH solvent. The 4.8 kcal/mol decrease in the C–H activation barrier height is close to the ΔG_{Solv} value of –5.3

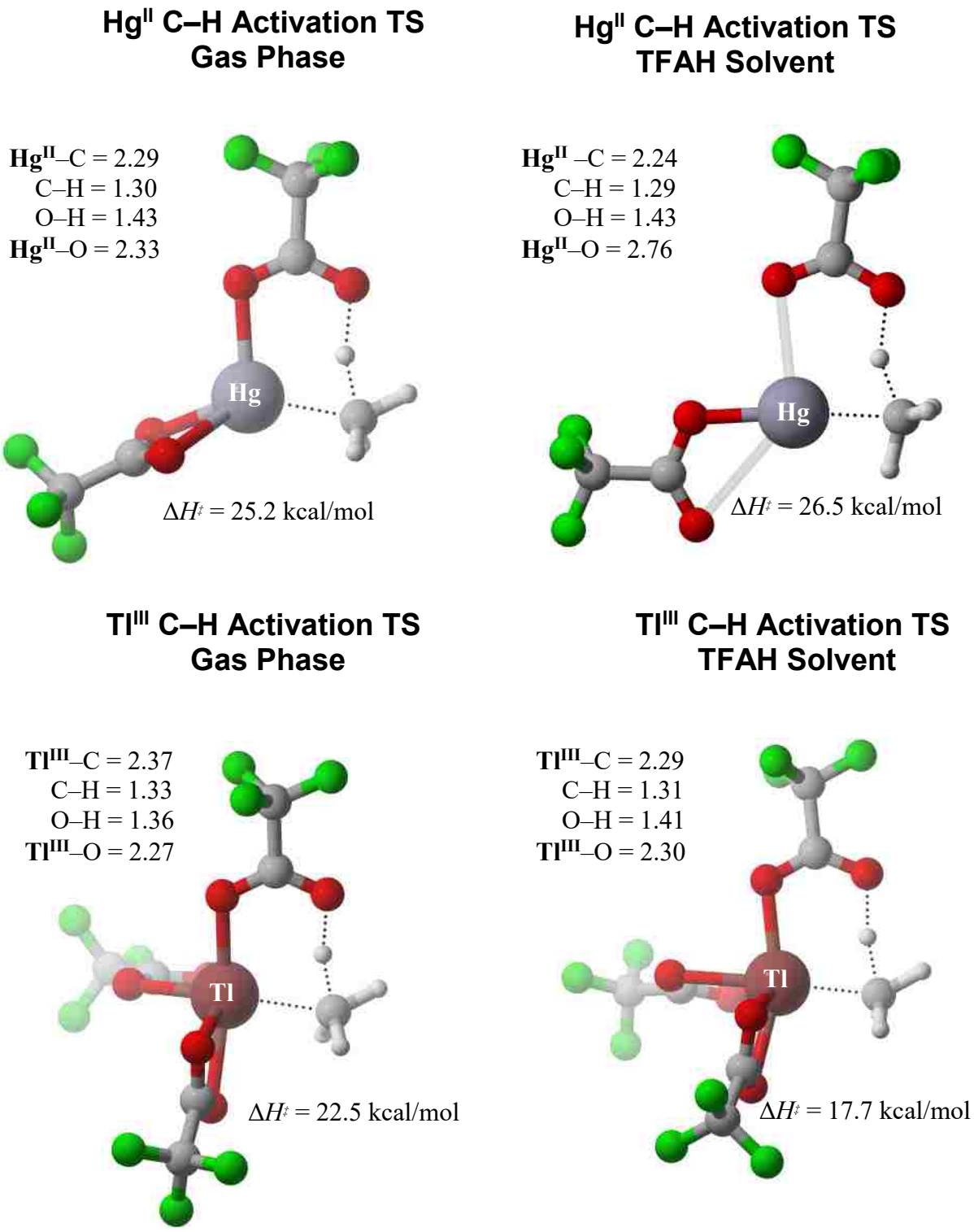

Figure 4-5. Gas phase and solvent optimized C–H activation transition state structures. (Å) kcal/mol (Table 4-3), further showing that the decrease in the C–H activation transition state barrier is due to slight solvation of the Tl^{III} C–H activation transition state complex. Furthermore,

the ΔG_{Solv} values along with the C–H activation barriers in the gas phase and in TFAH solvent illustrate that solvent indeed plays a critical role in the relative C–H activation barriers.

Table 4-3. ΔG_{Solv} values for $Tl^{III}(TFA)_3$ and the C–H activation transition state for $Tl^{III}(TFA)_3$ with methane. (kcal/mol)

	ΔG_{Solv}
$\mathbf{Tl^{III}}(TFA)_2$	–0.7
$\mathbf{Tl^{III}}(TFA)_3$ with methane C–H Activation Transition State	–5.3

Solvation effects are not the only effect that enhances the reactivity difference between Hg^{II} and Tl^{III}, there is also an intrinsic reactivity difference of $\Delta\Delta H^{\ddagger} \approx 3$ kcal/mol. This difference can be explained electrostatically and with frontier molecular orbital theory. From an electrostatic point of view, the intrinsic reactivity difference can be understood by the higher oxidation of Tl^{III}; the higher oxidation state of Tl^{III} contributes to a more stabilizing $M^{\delta+}$–$C^{\delta-}$ interaction and hence a lower C–H activation transition state. Alternatively, the intrinsic reactivity difference can also be explained by the frontier-orbitals displayed in Figure 4-2. The lower lying LUMO of Tl^{III} leads to a more stabilizing forward-bonding orbital interaction for Tl^{III} than Hg^{II}.

4.5 Conclusion

Calculations indicate that $Tl^{III}(TFA)_3$ activates alkanes by a C–H activation mechanism that is electronically dominated by stabilizing forward-bonding between the C–H σ orbital of the alkane interacting with the low energy 6s LUMO of Tl^{III}. This favorable interaction is decreased for EtTFA and raises the C–H activation barrier and prevents overoxidation. This orbital interaction, along with solvent effects, also rationalizes the fast reactivity of $Tl^{III}(TFA)_3$ and the lack of reactivity for $Hg^{II}(TFA)_2$. Comparison of low-spin $Ir^{III}(TFA)_3$ to $Tl^{III}(TFA)_3$ for C–H activation

and M–R functionalization revealed that the key to Tl^{III} oxidation of alkanes is a moderate barrier for C–H bond activation coupled with a very low barrier for M–R functionalization.

4.6 References

(1) Hashiguchi, B. G.; Konnick, M. M.; Bischof, S. M.; Gustafson, S. J.; Devarajan, D.; Gunsalus, N.; Ess, D. H.; Periana, R. A. *Science* **2014**, *343*, 1232.

(2) Ahlquist, M.; Periana, R. A.; Goddard III, W. A. *Chem. Commun.* **2009**, 2373.

(3) Gustafson, S. J.; Fuller, J. T.; Devarajan, D.; Snyder, J.; Periana, R. A.; Hashiguchi, B. G.; Konnick, M. M.; Ess, D. H. *Organometallics* **2015**, *34*, 5485.

(4) Hashiguchi, B. G.; Bischof, S. M.; Konnick, M. M.; Periana, R. A. *Acc. Chem. Res.* **2012**, *45*, 885.

(5) Hashiguchi, B. G.; Hövelmann, C. H.; Bischof, S. M.; Lokare, K. S.; Leung, C. H.; Periana, R. A. In *Encyclopedia of Inorganic Chemistry*; John Wiley & Sons, Ltd: 2006.

(6) Konnick, M. M.; Bischof, S. M.; Yousufuddin, M.; Hashiguchi, B. G.; Ess, D. H.; Periana, R. A. *J. Am. Chem. Soc* **2014**, *136*, 10085.

(7) Periana, R. A.; Taube, D. J.; Evitt, E. R.; Löffler, D. G.; Wentrcek, P. R.; Voss, G.; Masuda, T. *Science* **1993**, *259*, 340.

(8) Periana, R. A.; Taube, D. J.; Gamble, S.; Taube, H.; Satoh, T.; Fujii, H. *Science* **1998**, *280*, 560.

(9) Xu, Z.; Oxgaard, J.; Goddard, W. *Organometallics* **2008**, *27*, 3770.

(10) Zerella, M.; Bell, A. T. *J. Mol. Catal. A-Chem.* **2006**, *259*, 296.

(11) Zerella, M.; Kahros, A.; Bell, A. T. *J. Catal.* **2006**, *237*, 111.

(12) Zerella, M.; Mukhopadhyay, S.; Bell, A. T. *Chem. Commun.* **2004**, 1948.

(13) Mylvaganam, K.; Bacskay, G. B.; Hush, N. S. *J. Am. Chem. Soc* **1999**, *121*, 4633.

(14) Ouellette, R. J.; Kordosky, G.; Levin, C.; Williams, S. *J. Org. Chem.* **1969**, *34*, 4104.

(15) Ouellette, R. J.; Shaw, D. L.; South, A., Jr. *J. Am. Chem. Soc.* **1964**, *86*, 2744.

(16) Stolarov, I. P.; Vargaftik, M. N.; Shishkin, D. I.; Moiseev, I. I. *J. Chem. Soc., Chem. Commun.* **1991**, 938.

(17) Vargaftik, M. N.; Stolarov, I. P.; Moiseev, I. I. *J. Chem. Soc., Chem. Commun.* **1990**, 1049.

(18) Strassner, T.; Muehlhofer, M.; Zeller, A.; Herdtweck, E.; Herrmann, W. A. *J. Organomet. Chem.* **2004**, *689*, 1418.

(19) Sen, A. *Acc. Chem. Res.* **1998**, *31*, 550.

(20) Elson, I. H.; Kochi, J. K. *J. Am. Chem. Soc* **1973**, *95*, 5060.

(21) Lau, W.; Huffman, J. C.; Kochi, J. K. *J. Am. Chem. Soc* **1982**, *104*, 5515.

(22) Lau, W.; Kochi, J. K. *J. Am. Chem. Soc* **1984**, *106*, 7100.

(23) Lau, W.; Kochi, J. K. *J. Am. Chem. Soc* **1986**, *108*, 6720.

(24) King, C. R.; Gustafson, S. J.; Ess, D. H.; *in Computational Studies in Organometallic Chemistry* Springer Berlin Heidelberg: 2015, p 163.

(25) Ahlquist, M.; Nielsen, R. J.; Periana, R. A.; Goddard III, W. A. *J. Am. Chem. Soc* **2009**, *131*, 17110.

(26) Conley, B. L.; Tenn III, W. J.; Young, K. J. H.; Ganesh, S. K.; Meier, S. K.; Ziatdinov, V. R.; Mironov, O.; Oxgaard, J.; Gonzales, J.; Goddard III, W. A.; Periana, R. A. *J. Mol. Catal. A-Chem.* **2006**, *251*, 8.

(27) Golisz, S. R.; Gunnoe, B. T.; Goddard, W. A., III; Groves, J. T.; Periana, R. A. *Catal Lett* **2011**, *141*, 213.

(28) Webb, J. R.; Bolaño, T.; Gunnoe, T. B. *ChemSusChem* **2011**, *4*, 37.

(29) Allen, K. E.; Heinekey, D. M.; Goldman, A. S.; Goldberg, K. I. *Organometallics* **2013**, *32*, 1579.

(30) Pahls, D. R.; Allen, K. E.; Goldberg, K. I.; Cundari, T. R. *Organometallics* **2014**, *33*, 6413.

(31) Cundari, T. R.; Yoshikawa, A. *Journal of Computational Chemistry* **1998**, *19*, 902.

(32) Burke, P. J.; Matthews, R. W.; Gillies, D. G. *J. Organomet. Chem.* **1976**, *118*, 129.

(33) Fung, C. W.; Khorramdel-Vahed, M.; Ranson, R. J.; Roberts, R. M. G. *J. Chem. Soc. Perk. T. 2* **1980**, 267.

5 TL^{III}–ALKYL REDUCTIVE FUNCTIONALIZATION IN WATER

5.1 Introduction

Functionalization of alkane C–H bonds can occur by electrophilic C–H activation followed by metal–alkyl (M–R) functionalization.[1-4] While C–H activation has been extensively studied by experiment and theory,[5-20] there are a limited number of experimental and computational studies of M–R functionalization reactions, and most focus on transition metal complexes.[6,21-26] For example, Cundari used DFT calculations to show that the stronger the nucleophile, the lower the transition state barrier for carbon-heteroatom bond formation in Rh-alkyl complexes.[23,25,26] Other studies have emphasized the identity of the metal, metal charge, and ancillary ligands to stabilize electron density.[27]

Based on a combination of DFT calculations and experimental results, Tl^{III} acetate complexes in acid solvent (trifluoroacetic acid and acetic acid) are proposed to promote C–H bond functionalization via tandem C–H activation and M–R functionalization reactions.[28,29] This suggests the possibility that several previously reported examples of main-group M–R complexes might also undergo closed-shell two-electron reductive M–R functionalization reactions, which could be useful in the future design of alkane oxidation catalytic cycles based on main-group metals.

Kurosawa and Okawara reported an example of main-group metal M–R functionalization in water.[30-32] In this example, $(OAc)_2Tl^{III}(CH_3)$ was isolated from the reaction of $(OAc)Tl^{III}(CH_3)_2$ with $Hg(OAc)_2$ in methanol (Equation 5-1).[31] The isolated $(OAc)_2Tl^{III}(CH_3)$ product was then dissolved in water to give methyl acetate (MeOAc) and methanol (Equation 5-2).[32,33] In water the Tl^{III}–CH_3 bond undergoes a two-electron reduction to $Tl^{I}(OAc)$.[34] This M–R functionalization reaction proceeds slowly at room temperature and rapidly at elevated temperatures of ~100°C.[30-32] Glushkova and Kocheshkov reported a similar M–R functionalization reaction of diarylthallium acetates with thallium triacetate.[35]

$$(OAc)Tl^{III}(CH_3)_2 + Hg^{II}(OAc)_2 \xrightarrow[CH_3OH]{} (OAc)_2Tl^{III}(CH_3) + (OAc)Hg^{III}(CH_3) \qquad 5\text{-}1$$

$$(OAc)_2Tl^{III}(CH_3) \xrightarrow[H_2O]{} (OAc)Tl^{I} + CH_3OAc + CH_3OH + HOAc \qquad 5\text{-}2$$

One possible M–R functionalization mechanism involves methyl group transfer from $(OAc)Tl^{III}(CH_3)_2$ to $Tl^{III}(OAc)_3$ to form a short-lived $(OAc)_2Tl^{III}(CH_3)$ intermediate that is further functionalized (Scheme 5-1). Similar to the functionalization of $(OAc)Tl^{III}(CH_3)_2$, Hart and Ingold observed that $(X)Tl^{III}(R)_2$, where X = halide anions, results in alkyl halide products by reaction with thallium trihalides and no stable thallium monoalkyl intermediate was observed.[36,37]

Scheme 5-1. Proposed reaction pathway for M–R functionalization of $(OAc)Tl^{III}(CH_3)_2$ with $Tl^{III}(OAc)_3$ in water.

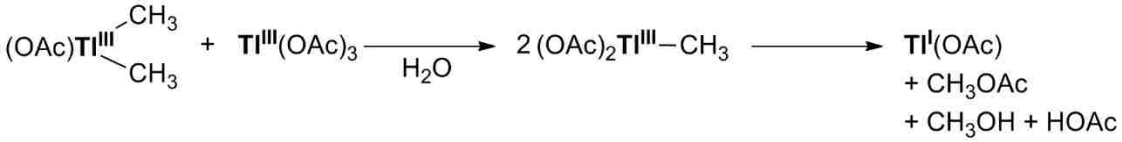

The remainder of this chapter reports a detailed density functional theory (DFT) study of the mechanism of methyl group transfer from $(OAc)Tl^{III}(CH_3)_2$ to $Tl^{III}(OAc)_3$ and subsequent M–R functionalization in water.

5.2 $(OAc)Tl^{III}(CH_3)_2$ Structure

There are several possible structures for $(OAc)Tl^{III}(CH_3)_2$ (Scheme 5-2). Experimental IR data of dialkyl thallium complexes indicate a possible mixture of mononuclear and dinuclear structures.[32,38,39] Scheme 5-2 shows a variety of structures that were calculated in a continuum of water solvent. The lowest energy structure corresponds to structure B where the two mononuclear fragments are weakly coordinated by nonbonding electron pairs from the acetate ligands. The ΔH for B is –15.5 kcal/mol and ΔG = –1.5 kcal/mol relative to two separated $(OAc)Tl^{III}(CH_3)_2$ structures (Scheme 5-2A). Structure D is commonly proposed,[30,35] but the ΔH for this structure is ~5 kcal/mol higher in enthalpy than B and the ΔG is slightly endergonic. No stable structures for C and E were located. These results suggest that there is a combination of the mononuclear and dinuclear structures in solution. This is consistent with NMR studies that show that $(CH_3)_2Tl^{III}OH$ is composed of 10% dinuclear, 36% mononuclear, and 54% of the $[(CH_3)_2Tl^{III}(H_2O)_x]^+$ cation.[40,41]

Scheme 5-2. Mononuclear and dinuclear $(OAc)Tl^{III}(CH_3)_2$ structures examined.

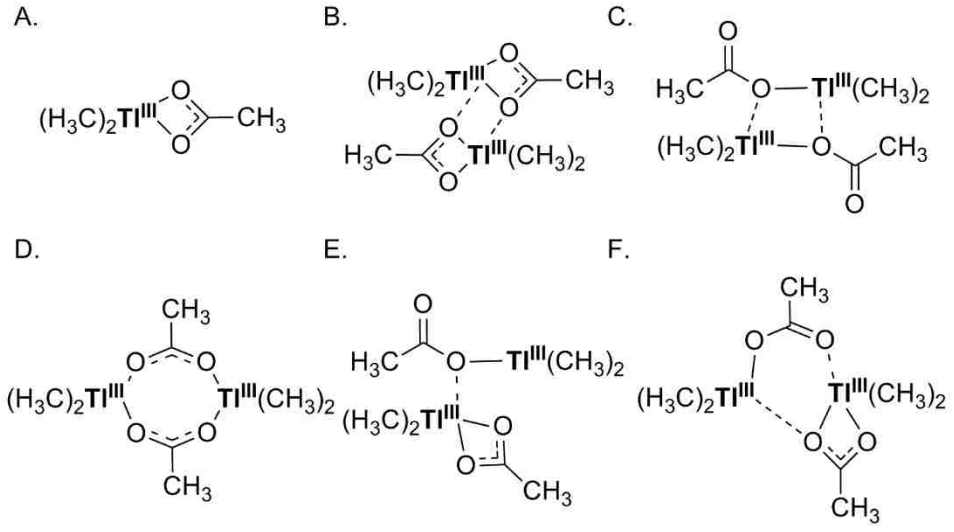

In addition to consideration of nuclearity, dialkylthallium complexes have also been shown to be weak acids when dissolved in water. Water has been proposed to weakly coordinate to a cationic dialkyl complex.[42] Therefore, the energetics of cationic complexes for dialkylthallium acetate were examined. Scheme 5-3 shows the calculated energies for acetate dissociation from $(OAc)Tl^{III}(CH_3)_2$ with and without explicit water coordination. Without water coordination, the ΔH for $[Tl^{III}[(CH_3)_2]^+$ is –3.2 kcal/mol (ΔG = –5.4) . Modeling the $[(OAc)Tl^{III}(CH_3)_2]^+$ with a water molecule is slightly more exothermic to form $[(H_2O)Tl^{III}[(CH_3)_2]^+$ (ΔH = –11.4 kcal/mol). Based on experimental studies,[40,41] and these calculated energies, mononuclear neutral and cationic pathways were examined.

Scheme 5-3. Energies for formation of $[Tl^{III}(CH_3)_2]^+$.

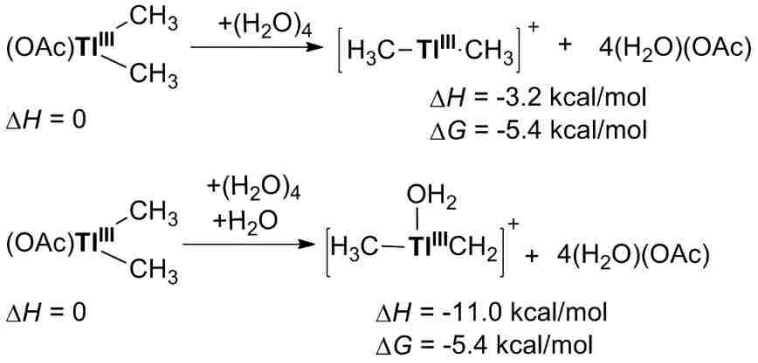

5.3 Mechanism for Methyl Group Transfer from $(OAc)Tl^{III}(CH_3)_2$ to $Tl^{III}(OAc)_3$

As indicated in the introduction, reaction of $(OAc)Tl(CH_3)_2$ leads to MeOAc and methanol in the presence of $Tl^{III}(OAc)_3$. This suggests the possibility of methyl group transfer from $(OAc)Tl^{III}(CH_3)_2$ to $Tl^{III}(OAc)_3$ to form a transient $(OAc)_2Tl^{III}(CH_3)$ species followed by M–R reductive functionalization. Pathways were explored for the direct intramolecular and intermolecular functionalization of $(OAc)Tl^{III}(CH_3)_2$ and alkyl group transfer followed by M–R functionalization.

5.3.1 $(OAc)Tl^{III}(CH_3)_2$ and $[Tl^{III}(CH_3)_2]^+$ Bond Strength and No M–R Functionalization

The Tl^{III}–C bonds in dialkyl thallium complexes are relatively stable in water.[32,41] Homolytic and heterolytic Tl^{III}–C bond strengths were calculated along with barriers for reductive elimination and reductive M–R functionalization to examine this stability. Homolysis of one of the Tl^{III}–CH_3 bonds in $(OAc)Tl^{III}(CH_3)_2$ requires ΔH = 44.3 kcal/mol. Homolysis of a Tl^{III}–CH_3 bond for $[Tl^{III}[(CH_3)_2]^+$ requires ΔH = 38.0 (Table 5-1). The Tl^{III}–OAc homolysis bond enthalpy is 91.2 kcal/mol for $(OAc)Tl^{III}(CH_3)_2$. Heterolysis of the Tl^{III}–CH_3 bond in $(OAc)Tl^{III}(CH_3)_2$ to the Tl^{III} cation and methyl anion requires $\Delta H \sim 90$ kcal/mol. This indicates that the Tl^{III}–C bond is relatively covalent for the dialkyl thallium complex.

Table 5-1. Homolytic and heterolytic bond energies for $(OAc)Tl^{III}(CH_3)_2$ and the $[Tl^{III}(CH_3)_2]^+$ cation. (kcal/mol; X=OAc)

	$[(X)\mathbf{Tl^{III}}(CH_3)]^+ + CH_3^-$	$[(X)\mathbf{Tl^{III}}(CH_3)]^- + CH_3^+$	$[(X)\mathbf{Tl^{III}}(CH_3)]^\bullet + CH_3^\bullet$	$[\mathbf{Tl^{III}}(CH_3)_2]^\bullet + X^\bullet$	$[\mathbf{Tl^{III}}(CH_3)_2]^+ + X^-$
$(X)\mathbf{Tl^{III}}(CH_3)_2$	90.2	106.5	44.3	91.2	29.1

	$[\mathbf{Tl^{III}}(CH_3)]^{2+} + CH_3^-$	$\mathbf{Tl^{III}}(CH_3) + CH_3^+$	$[\mathbf{Tl^{III}}(CH_3)]^{+\bullet} + CH_3^\bullet$
$[\mathbf{Tl^{III}}(CH_3)_2]^+$	140.6	88.0	38.0

Alternative to Tl^{III}–C bond cleavage, there is also the possibility of C–C and C–O bond reductive elimination and M–R functionalization (Scheme 5-4). The ΔH for C–C reductive elimination to form ethane and $Tl^{I}(OAc)$ is 66.4 kcal/mol. The ΔH for C–O reductive elimination to give methyl acetate and $Tl^{I}(CH_3)$ is 62.0 kcal/mol. The relatively large enthalpy changes for reductive elimination and functionalization indicates that $(OAc)Tl^{III}(CH_3)_2$ and $[Tl^{III}[(CH_3)_2]^+$ are too electron rich to allow a two-electron reduction process.

Nucleophilic attack by water (S_N2) on the Tl^{III}–C bond leads to methanol and $(AcOH)Tl^{III}(CH_3)$ (Scheme 5-4C). The activation barrier for this transition state is 49.0 kcal/mol and 42.0 kcal/mol with a second explicit water. Overall, the ~40 kcal/mol Tl^{III}–C homolytic bond strength and > 40 kcal/mol S_N2 barrier indicates that in water $(OAc)Tl^{III}(CH_3)_2$ does not undergo direct M–R functionalization. Likewise, the large barrier for dissociation and nucleophilic attack of OAc on the Tl^{III}–C bond (Scheme 5-4D) is also not feasible with a barrier of ΔH = 46.3 kcal/ mol.

Scheme 5-4. Possible reductive elimination and M–R functionalization transition states.

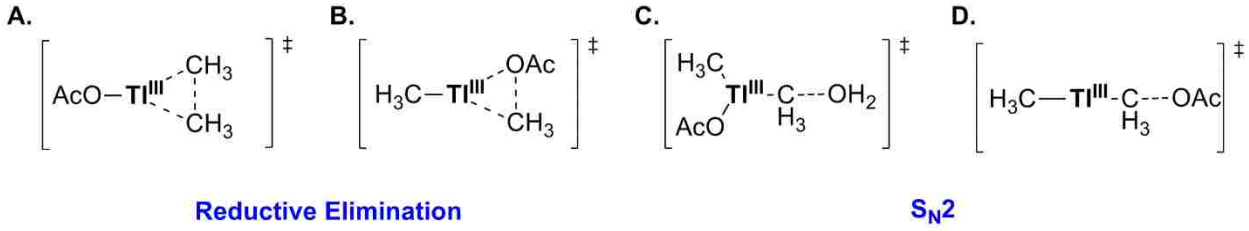

5.3.2 Open-Shell Pathways

The open-shell pathways in were investigated.[43-46] Electron transfer (ET) of one electron from $(OAc)Tl^{III}(CH_3)_2$ to $Tl^{III}(OAc)_3$ requires 50.0 kcal/mol. As expected, ET from cationic dialkyl complexes to $Tl^{III}(OAc)_3$ is much more endothermic and requires > 100 kcal/mol. Alternatively, a Proton-coupled ET (PCET) pathway was also examined.[48] While slightly lower in energy it still requires > 40 kcal/mol and is not viable.

Another open-shell pathway is hydrogen atom transfer. Unfortunately, all attempts to locate the $[(OAc)_3Tl^{II}(H)]^{\bullet}$ structure failed.

Table 5-2. Energetics for open-shell pathways. (kcal/mol)

	ET		PCET
	$[(OAc)\mathbf{Tl^{II}}(CH_3)_2]^{-\bullet}$ + $[\mathbf{Tl^{II}}(OAc)_3]^{+\bullet}$	$[(OAc)\mathbf{Tl^{II}}(CH_3)_2]^{+\bullet}$ + $[\mathbf{Tl^{II}}(OAc)_3]^{-\bullet}$	$[\mathbf{Tl^{II}}(CH_3)(CH_2OAc)]^{\bullet}$ + $[\mathbf{Tl^{II}}(OAc)_2(AcOH)]^{\bullet}$
$(OAc)\mathbf{Tl^{III}}(CH_3)_2$ + $\mathbf{Tl^{III}}(OAc)_3$	125.0	50.5	41.8
	$[\mathbf{Tl^{II}}(CH_3)_2]^{\bullet}$ + $[\mathbf{Tl^{III}}(OAc)_3]^{+}$		$[\mathbf{Tl^{II}}(CH_3)(CH_2)]^{+\bullet}$ + $[\mathbf{Tl^{II}}(OAc)_2(AcOH)]^{\bullet}$
$[\mathbf{Tl^{III}}(CH_3)_2]^{+}$+ $\mathbf{Tl^{III}}(OAc)_3$	105.8		41.8

5.3.3 Hydride Abstraction and Proton Transfer

Table 5-3. Energetics for proton transfer from the Dialkylthallium to $Tl^{III}(OAc)_3$. (kcal/mol)

	Hydride Transfer	Proton Transfer
	$[(OAc)\mathbf{Tl^{III}}(CH_3)(CH_2)]^{+}$ + $[\mathbf{Tl^{III}}(OAc)_3H]^{-}$	$[(OAc)\mathbf{Tl^{III}}(CH_3)(CH_2]^{+}$ + $[\mathbf{Tl^{III}}(OAc)_2(AcOH)]^{+}$
$(OAc)\mathbf{Tl^{III}}(CH_3)_2$ + $\mathbf{Tl^{III}}(OAc)_3$	24.5	80.7
		$[\mathbf{Tl^{III}}(CH_3)(CH_2)]$ + $[\mathbf{Tl^{III}}(OAc)_2(AcOH)]^{+}$
$[\mathbf{Tl^{III}}(CH_3)_2]^{+}$ + $\mathbf{Tl^{III}}(OAc)_3$		67.3

Hydride abstraction and proton transfer mechanisms were also investigated (Table 5-1). Hydride transfer from $(OAc)Tl^{III}(CH_3)_2$ to $Tl^{III}(OAc)_3$ to form $[(OAc)Tl^{III}(CH_3)(CH_2)]^{+}$ and $[(OAc)_3Tl^{III}(H)]^{-}$ is endothermic by 24.5 kcal/mol. Proton transfer from $(OAc)Tl^{III}(CH_3)_2$ to $Tl^{III}(OAc)_3$ to form $[(OAc)Tl^{III}(CH_3)(CH_2)]^{-}$ and $[(OAc)_2Tl^{III}(AcOH)]^{+}$ requires 80.2 kcal/mol. The only favorable hydride transfer was found between $(OAc)Tl^{III}(CH_3)_2$ and $[Tl^{III}(OAc)_2]^{+}$, which is exothermic by –10.7 kcal/mol. No transition state for this process has been located. However,

mass spectrometry analysis of dimethylthallium halide complexes revealed no thallium hydride species.[47]

5.3.4 Alkyl Transfer

$(OAc)_2Tl^{III}(CH_3)$ can be formed through alkyl transfer from $(OAc)Tl^{III}(CH_3)_2$ to $Tl^{III}(OAc)_3$ via either a one-step or multi-step mechanism.[32,48] Scheme 5-5 and Scheme 5-6 illustrate possible pathways for the stepwise mechanism of alkyl transfer. Acetate dissociation from $Tl^{III}(OAc)_3$ followed by nucleophilic attack to the Tl^{III}–C bond of $(OAc)Tl^{III}(CH_3)_2$ (or $[Tl^{III}(CH_3)_2]^+$) requires an unfavorable ΔH = 57.5 kcal/mol and 39.0 kcal/mol for the cationic system (the neutral pathway is in Scheme 5-5B and the cationic pathway is in Scheme 5-6B) without explicit solvation.

Scheme 5-5. Methyl transfer pathways from $(OAc)Tl^{III}(CH_3)_2$ to $Tl^{III}(OAc)_3$. (kcal/mol)

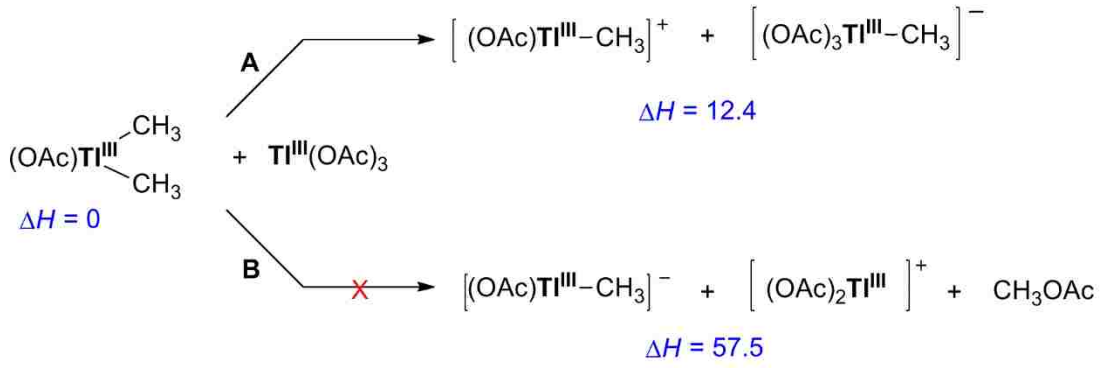

Scheme 5-6. Methyl transfer pathways from $[Tl^{III}(CH_3)_2]^+$ to $Tl^{III}(OAc)_3$. (kcal/mol)

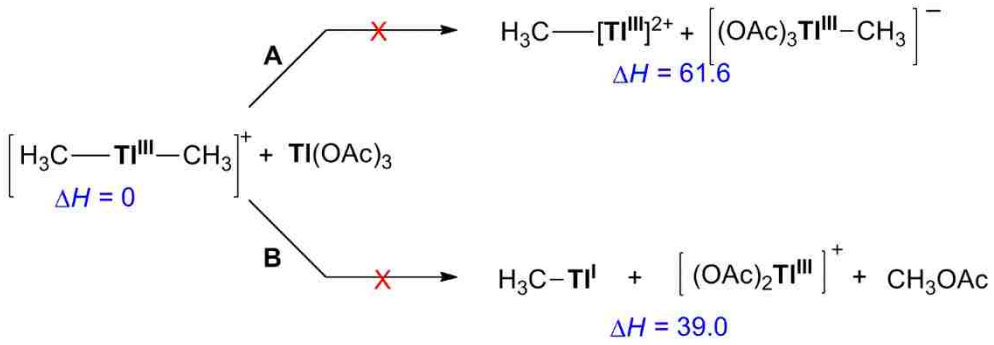

Scheme 5-7. Methyl transfer featuring simultaneous ligand transfer between neutral and cationic thallium dialkyl complex and $Tl^{III}(OAc)_3$. (kcal/mol)

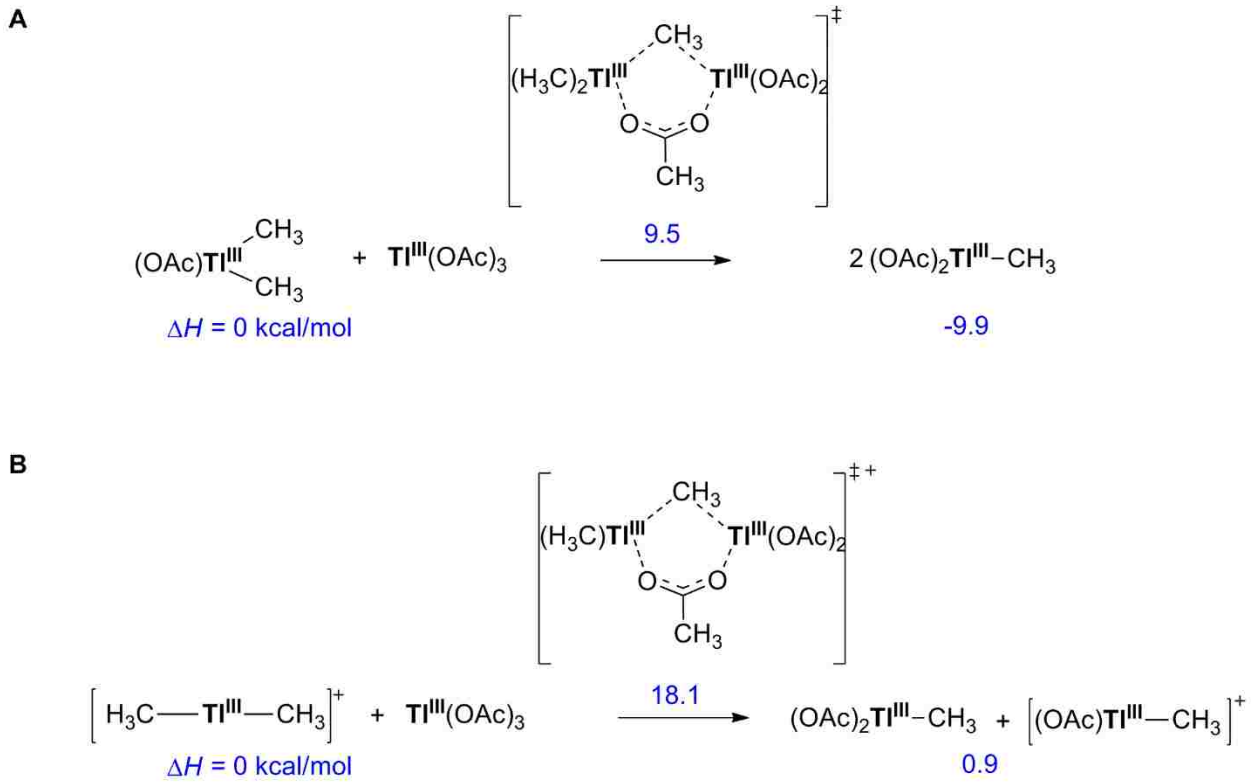

Methyl anion transfer from $(OAc)Tl^{III}(CH_3)_2$ to $Tl^{III}(OAc)_3$ results in the cation/anion pair $[(OAc)Tl^{III}(CH_3)]^+/[(OAc)_3Tl^{III}(CH_3)]^-$ (Scheme 5-5A) and is 12.4 kcal/mol endothermic. Despite extensive searching, it was not possible to locate a transition state for methyl group transfer between Tl^{III} metal centers with no ligand bridging or second ligand transfer. Methyl anion transfer from the Tl^{III} cation is unfavorable (ΔH = 61.6 kcal/mol, Scheme 5-6B). Alternatively, methyl anion transfer can take place with a simultaneous OAc ligand transfer (Scheme 5-7). Figure 5-1. shows the transition-state structure for this ligand exchange reaction. IRC calculations confirm that both the methyl group and OAc ligand are transferred; however, the IRC indicates that methyl group transfer may precede acetate ligand transfer in an asynchronous process. The activation enthalpy for ligand exchange is $\Delta H^{\ddagger}$ = 9.5 kcal/mol. There is also the possibility of ligand exchange between the $[Tl^{III}(CH_3)_2]^+$ cation and $Tl^{III}(OAc)_3$. The barrier for this transition state is $\Delta H^{\ddagger}$ = 18.1

kcal/mol from the $[Tl^{III}(CH_3)_2]^+$ cation and $Tl^{III}(OAc)_3$ ground states, which indicates that the cationic pathway is less likely than the neutral pathway.

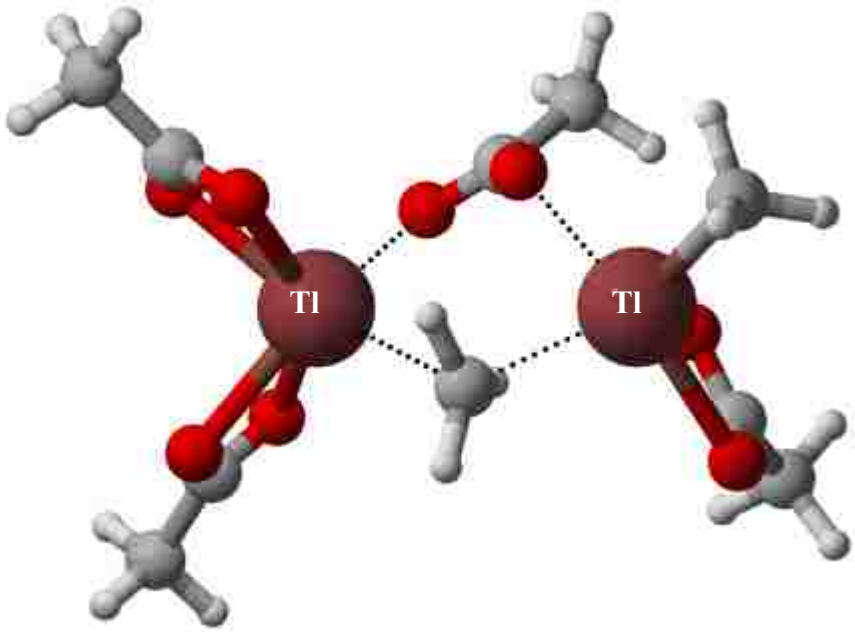

Figure 5-1. Concerted transition state for methyl and acetate ligand exchange between $(OAc)Tl^{III}(CH_3)_2$ and $Tl^{III}(OAc)_3$. (Å)

5.4 Functionalization of $(OAc)_2Tl^{III}(CH_3)$

In contrast to dialkyl thallium compounds, monoalkylthallium compounds quickly functionalize to form products.[30,32,35,41,49] For example, Hart and Ingold detected only products for the reaction of $(X)Tl^{III}(R)_2$ with $Tl^{III}(X)_3$ (where X = halides) without detecting the monoalkyl intermediate.[36]

Significant differences between the monoalkylthallium and dialkylthallium complexes are noticeable in the homolytic and heterolytic bond strengths (Table 5-1 and Table 5-4). The Tl^{III}–C bond homolytic bond strength for the monoalkylthallium compound increases by ~16 kcal/mol compared to the dialkylthallium Tl^{III}–C bond. Additionally, while the dialkylthallium complex favors methyl anion heterolysis, the monoalkylthallium complex favors methyl cation heterolysis.

Table 5-4. Homolytic and heterolytic bond energies of $(OAc)_2Tl^{III}(CH_3)$. (kcal/mol; X= OAc)

	$[(X)_2Tl^{III}]^+ + CH_3^-$	$[(X)_2Tl^{III}]^- + CH_3^+$	$[(X)_2Tl^{II}]^\bullet + CH_3^\bullet$	$[(X)Tl^{II}(CH_3)]^\bullet + AcO^\bullet$	$[(X)Tl^{III}(CH_3)]^+ + AcO^-$
$(X)_2Tl^{III}(CH_3)_2$	115.4	68.9	50.3	60.6	39.9

Scheme 5-8. Functionalization pathways of $(OAc)_2Tl^{III}(CH_3)$.

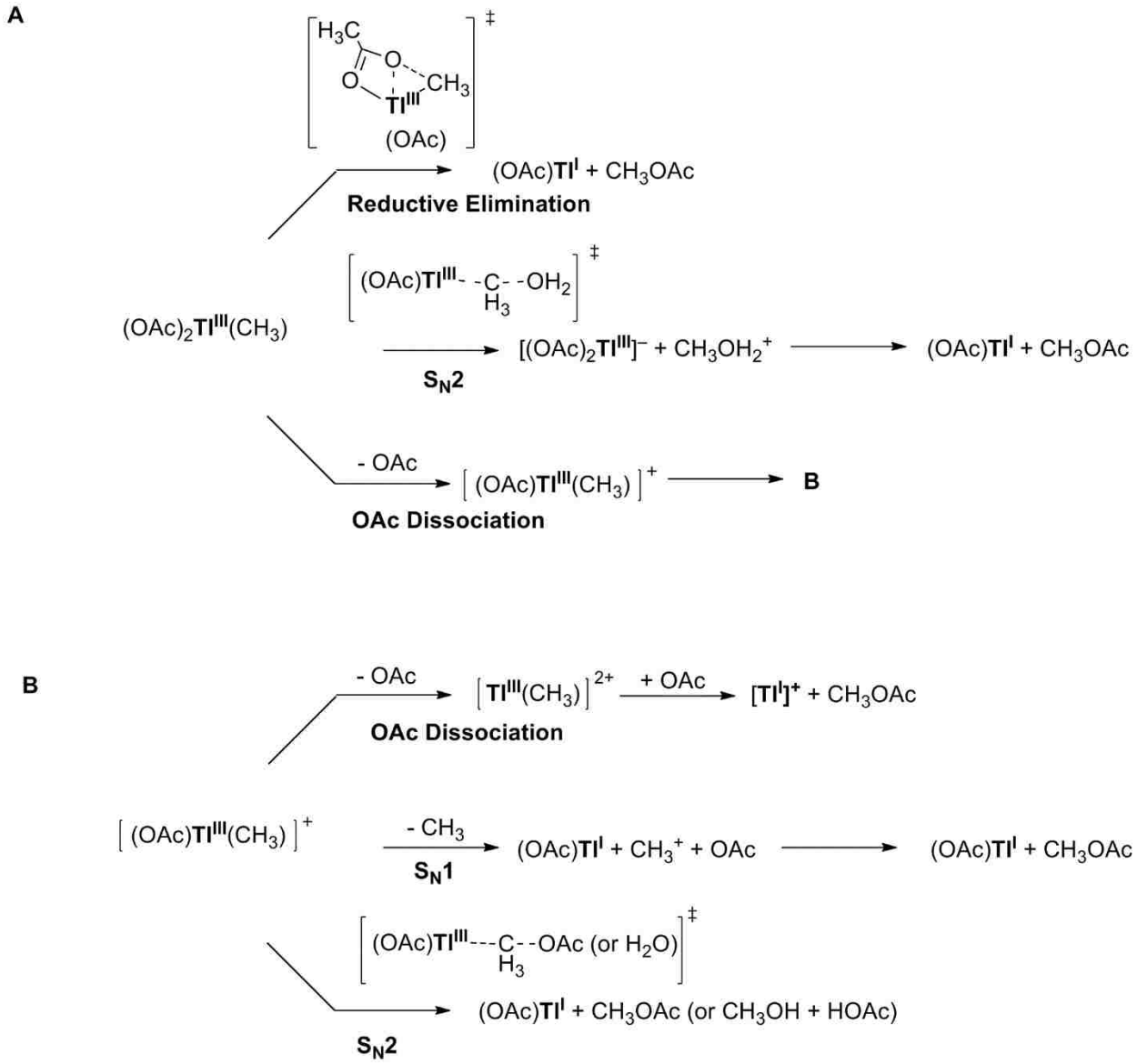

M–R functionalization can occur through several initial steps: (1) reductive elimination to form the MeOAc and $Tl^I(OAc)$; (2) S_N2 attack with water at the Tl^{III}–C bond of the neutral

monoalkylthallium complex (Scheme 5-8A), ane (3) acetate dissociation from the neutral monoalkylthallium complex.

Following dissociation of acetate there is the possibility of dissociation of a second acetate and an S_N1 pathway where a methyl cation forms from Tl^{III}–C bond heterolysis and then combines with acetate or water, and S_N2 attack with the free OAc ligand or water (Scheme 5-8A).

From $(OAc)_2Tl^{III}(CH_3)$ unfavorable pathways include reductive elimination and dissociation of both acetate ligands. The ΔH for reductive elimination is 43.2 kcal/mol. Dissociation of an acetate ligand is more favorable than dissociation of a methyl ligand (Table 5-4). Adding explicit water molecules, the ΔH for acetate dissociation is 31.3 kcal/mol for $[(H_2O)_5][(OAc)_2Tl^{III}(CH_3)]$ (Scheme 5-9). Dissociation of the second acetate ligand[41] is unfavorable at ΔH = 54.7. This is consistent with Pohl and Huber's rate calculations.[33]

Scheme 5-9. Dissociation of acetate anion. (kcal/mol)

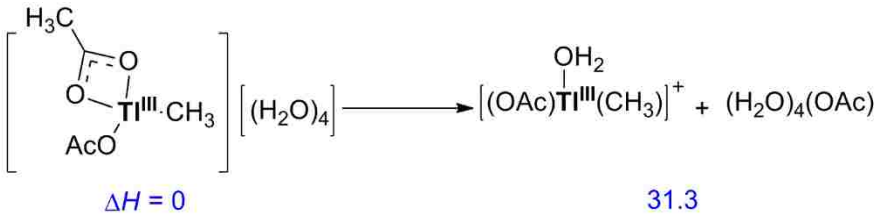

5.4.1 S_N2 Functionalization Pathways

There are several pathways for nucleophilic attack with both water and acetate to the Tl^{III}–C bond. The first is a backside nucleophilic attack of one of the carbon bonds with the neutral dialkylthallium complex with water. The barrier from this reaction is lower (ΔH = 25.7 kcal/mol) than the thermodynamics for acetate loss, but the thermodynamics for the products are endergonic (Scheme 5-10).

Scheme 5-10. Nucleophilic attack with water to the Tl^{III}–C bond of the neutral monoalkylthallium complex. (kcal/mol)

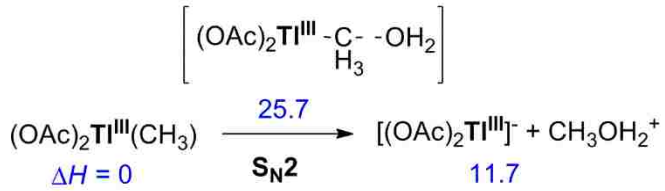

M–R functionalization of the thallium monocation, $[(OAc)Tl^{III}(CH_3)]^+$ is also thermodynamically accessible. The activation enthalpy for an S_N2 transition state with OAc and the cationic monoalkylthallium complex requires ΔH = 29.7 kcal/mol from the $[(OAc)Tl^{III}(CH_3)]^+$ intermediate. Alternatively, water can act as the nucleophile with a barrier of 18.5 kcal/mol from the $[(OAc)Tl^{III}(CH_3)]^+$ intermediate. Direct comparison of the acetate and H_2O nucleophiles was done using the explicitly solvated acetate complex $[(OAc)(H_2O)_4]^-$ where either acetate or water can act as a nucleophile In this case, the transition states for nucleophilic attack with acetate and water have only a 0.4 kcal/mol enthalpy difference suggesting these pathways are competitive.

5.4.2 S_N1 Functionalization Pathways of $[(OAc)Tl^{III}(CH_3)]^+$

The estimate for Tl^{III}–C bond heterolysis to form methyl cation $[(OAc)Tl^{III}(CH_3)]^+$ is ΔH = 42.4 kcal/mol without explicit solvent. Explicit solvent has a dramatic effect on this bond heterolysis energy. Addition of explicit solvent decreases the ΔH to –3.2 kcal/mol (Scheme 5-11). Importantly, this Tl^{III}–C bond heterolysis enthalpy estimate is competitive with nucleophilic substitution barriers (Scheme 5-10). A free energy barrier for the S_N1 transition state, obtained by QM/MD methods, is needed to more accurately compare these pathways.[50] Pohl and Huber have suggested that an S_N1 pathway is less likely than an S_N2 pathway because the addition of NaOAc to $(OAc)_2Tl^{III}(CH_3)$ decreased the rate of M–R functionalization.[33] However, it is possible that added acetate coordinates to Tl^{III} and reduces the rate of Tl^{III}–C bond heterolysis due to a decreased two-electron potential.

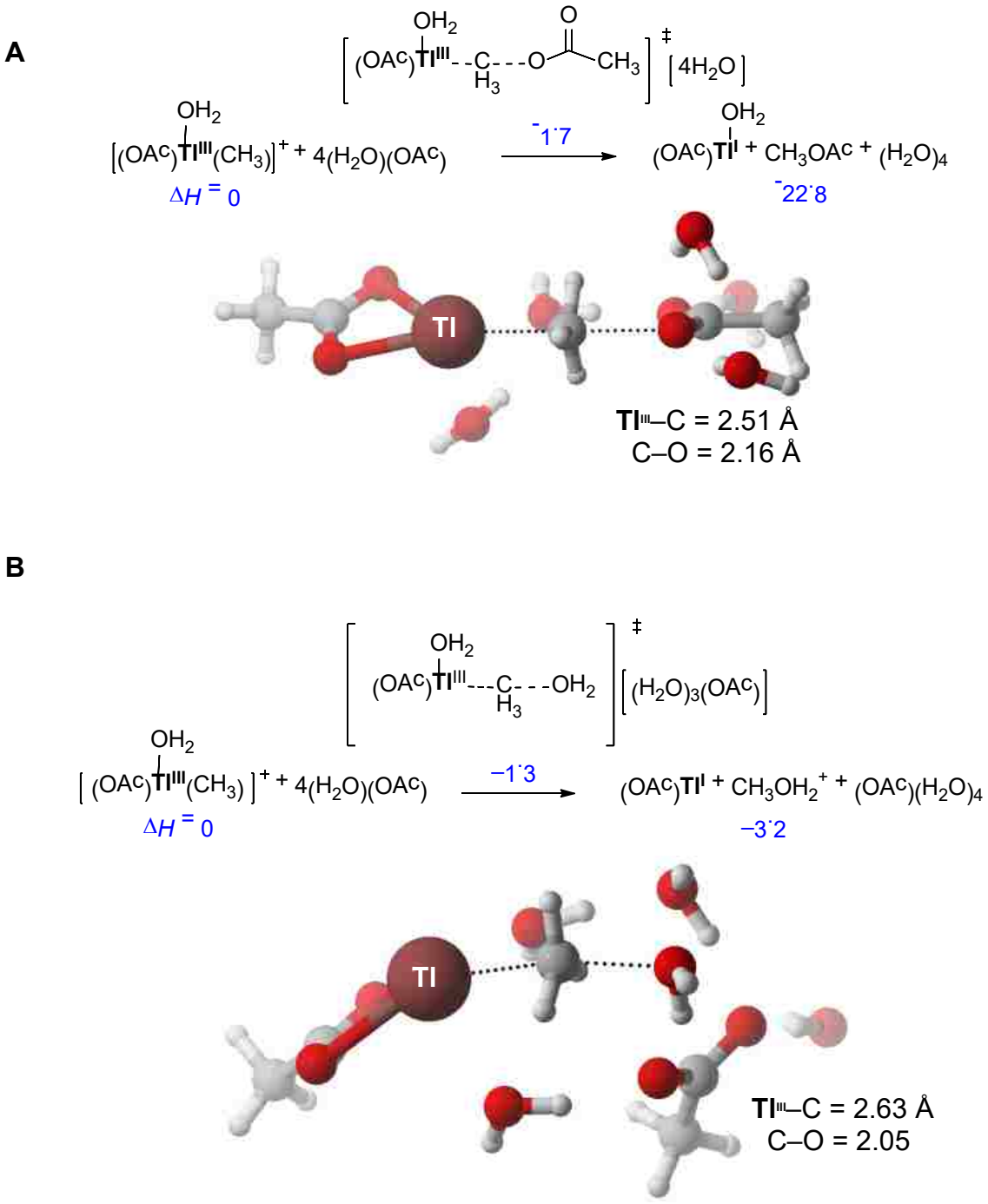

Figure 5-2. S_N2 M–R functionalization transition states. (kcal/mol)

Scheme 5-11. Methyl dissociation from $[(OAc)Tl^{III}(CH_3)]^+$ with and without explicit solvent. (kcal/mol)

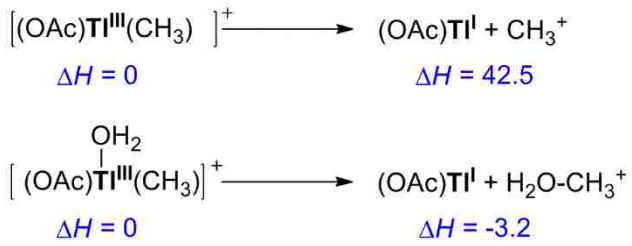

5.5 Conclusion

CH_3OAc, CH_3OH, AcOH, and $Tl^{III}(OAc)$ are formed from the reaction of $Tl^{III}(OAc)_3$ and $(OAc)Tl^{III}(CH_3)$. Calculations indicate that the reaction begins with an exchange of methyl and acetate groups to form $(OAc)_2Tl^{III}(CH_3)$. Subsequent acetate dissociation then provides a reroute to fast M–R functionalization by competitive water/acetate nucleophilic substitution at the Tl^{III}–C bond. These calculations cannot rule out the possibility of Tl^{III}–C bond heterolysis. Future molecular dynamics studies will likely be able to differentiate these pathways.

5.6 References

(1) Goldberg, K. I.; Goldman, A. S. *Activation and Functionalization of C–H Bonds*; American Chemical Society, 2004; Vol. 885.

(2) Crabtree, R. H. *Chem. Rev.* **1985**, *85*, 245.

(3) Crabtree, R. H. *Chem. Rev.* **1995**, *95*, 987.

(4) Crabtree, R. H. *J. Chem. Soc., Dalton Trans.* **2001**, 2437.

(5) Ahrens, S.; Zeller, A.; Taige, M.; Strassner, T. *Organometallics* **2006**, *25*, 5409.

(6) Burk, M. J.; Crabtree, R. H. *J. Am. Chem. Soc* **1987**, *109*, 8025.

(7) Chen, H.; Schlecht, S.; Semple, T. C.; Hartwig, J. F. *Science* **2000**, *287*, 1995.

(8) Choi, J.; MacArthur, A. H. R.; Brookhart, M.; Goldman, A. S. *Chem. Rev.* **2011**, *111*, 1761.

(9) Goldman, A. S.; Roy, A. H.; Huang, Z.; Ahuja, R.; Schinski, W.; Brookhart, M. *Science* **2006**, *312*, 257.

(10) Gol'dshleger, N. F.; Es'kova, V. V.; Shilov, A. E.; A.A., S. *Russ. J. Phys. Chem.* **1972**, *46*, 785.

(11) Gol'dshleger, N. F.; Moravsky, A. P. *Usp. Khim.* **1994**, *63*, 130.

(12) Haibach, M. C.; Kundu, S.; Brookhart, M.; Goldman, A. S. *Acc. Chem. Res.* **2012**, *45*, 947.

(13) Hartwig, J. F. *Acc. Chem. Res.* **2012**, *45*, 864.

(14) Hartwig, J. F.; Cook, K. S.; Hapke, M.; Incarvito, C. D.; Fan, Y.; Webster, C. E.; Hall, M. B. *J. Am. Chem. Soc* **2005**, *127*, 2538.

(15) Muehlhofer, M.; Strassner, T.; Herrmann, W. A. *Angew. Chem. Int. Ed.* **2002**, *41*, 1745.

(16) Periana, R. A.; Mironov, O.; Taube, D.; Bhalla, G.; Jones, C. J. *Science* **2003**, *301*, 814.

(17) Periana, R. A.; Taube, D. J.; Gamble, S.; Taube, H.; Satoh, T.; Fujii, H. *Science* **1998**, *280*, 560.

(18) Stolarov, I. P.; Vargaftik, M. N.; Shishkin, D. I.; Moiseev, I. I. *J. Chem. Soc., Chem. Commun.* **1991**, 938.

(19) Strassner, T.; Muehlhofer, M.; Zeller, A.; Herdtweck, E.; Herrmann, W. A. *J. Organomet. Chem.* **2004**, *689*, 1418.

(20) Vargaftik, M. N.; Stolarov, I. P.; Moiseev, I. I. *J. Chem. Soc., Chem. Commun.* **1990**, 1049.

(21) Cundari, T. R.; Grimes, T. V.; Gunnoe, T. B. *J. Am. Chem. Soc* **2007**, *129*, 13172.

(22) Figg, T. M.; Cundari, T. R.; Gunnoe, T. B. *Organometallics* **2011**, *30*, 3779.

(23) Figg, T. M.; Webb, J. R.; Cundari, T. R.; Gunnoe, T. B. *J. Am. Chem. Soc* **2012**, *134*, 2332.

(24) Mei, J.; Carsch, K. M.; Freitag, C. R.; Gunnoe, T. B.; Cundari, T. R. *J. Am. Chem. Soc* **2013**, *135*, 424.

(25) O'Reilly, M. E.; Pahls, D. R.; Cundari, T. R.; Gunnoe, T. B. *Organometallics* **2014**, *33*, 6504.

(26) Pahls, D. R.; Groves, J. T.; Gunnoe, T. B.; Cundari, T. R. *Organometallics* **2014**, *33*, 1936.

(27) Yoh, S.-D.; Cheong, D.-Y.; Lee, O.-S. *J. Phys. Org. Chem.* **2003**, *16*, 63.

(28) Gustafson, S. J.; Fuller, J. T.; Devarajan, D.; Snyder, J.; Periana, R. A.; Hashiguchi, B. G.; Konnick, M. M.; Ess, D. H. *Organometallics* **2015**, *34*, 5485.

(29) Hashiguchi, B. G.; Konnick, M. M.; Bischof, S. M.; Gustafson, S. J.; Devarajan, D.; Gunsalus, N.; Ess, D. H.; Periana, R. A. *Science* **2014**, *343*, 1232.

(30) Kurosawa, H.; Okawara, R. *J. Organomet. Chem.* **1967**, *10*, 211.

(31) Kurosawa, H.; Okawara, R. *J. Inorg. Nucl. Chem.* **1967**, *3*, 93.

(32) Kurosawa, H.; Okawara, R. *Trans. N. Y. Acad. Sci.* **1968**, *30*, 962.

(33) Pohl, U.; Huber, F. *J. Organomet. Chem.* **1976**, *116*, 141.

(34) Mckillop, A.; Taylor, E. C. In *Organic Syntheses by Oxidation with Metal Compounds*; Mijs, W. J., de Jonge, C. R. H. I., Eds.; Springer US: Boston, MA, 1986, p 695.

(35) Kurosawa, H.; Okawara, R. *Organomet. Chem. Rev. A* **1970**, *6*, 65.

(36) Hart, C. R.; Ingold, C. K. *J. Chem. Soc.* **1964**, 4372.

(37) Pohl, U.; Huber, F. *Z. Naturforsch. B Chem. Sci.* **1978**, *33*, 1188.

(38) Kurosawa, H.; Okawara, R. *J. Organomet. Chem.* **1969**, *19*, 253.

(39) Kurosawa, H.; Yasuda, K.; Okawara, R. *Bull. Chem. Soc. Jpn.* **1967**, *40*, 861.

(40) Lawrence, J. K.; Prue, J. E. *J. Solution Chem.*, **1974**,*3*, 553.

(41) Lee, A. G. *Q. Rev. Chem. Soc.* **1970**, *24*, 310.

(42) Beletskaya, I. P.; Butin, K. P.; Ryabtsev, A. N.; Reutov, O. A. *J. Organomet. Chem.* **1973**, *59*, 1.

(43) Elson, I. H.; Kochi, J. K. *J. Am. Chem. Soc* **1973**, *95*, 5060.

(44) Lau, W.; Huffman, J. C.; Kochi, J. K. *J. Am. Chem. Soc* **1982**, *104*, 5515.

(45) Lau, W.; Kochi, J. K. *J. Am. Chem. Soc* **1984**, *106*, 7100.

(46) Lau, W.; Kochi, J. K. *J. Am. Chem. Soc* **1986**, *108*, 6720.

(47) Lee, A. G. *Int. J. Mass. Spectrom. Ion. Phys.* **1969**, *3*, 239.

(48) Abraham, M. H.; Hill, J. A. *J. Organomet. Chem.* **1967**, *7*, 11.

(49) Lee, A. G. *J. Chem. Soc. A.* **1970**, 467.

(50) Ruff, F.; Farkas, Ö. *J. Phys. Org. Chem.* **2008**, *21*, 53.